

Article

Long-Term Variation of Runoff Coefficient during Dry and Wet Seasons Due to Climate Change

Doan Thi Thu Ha, Mona Ghafouri-Azar  and Deg-Hyo Bae * 

Department of Civil & Environmental Engineering, Sejong University, 98 Gunja-Dong, Gwangjin-Gu, Seoul 143-747, Korea; doanha@imh.ac.vn (D.T.T.H.); mga@sju.ac.kr (M.G.-A.)

* Correspondence: dhbae@sejong.ac.kr; Tel.: +82-2-3408-3814

Received: 12 October 2019; Accepted: 15 November 2019; Published: 17 November 2019



Abstract: This study investigates the future long-term variation of the runoff coefficient during dry and wet seasons in five major basins in South Korea. The variation is estimated from the Soil and Water Assessment Tool (SWAT) model outputs based on an ensemble of 13 different Coupled Model Intercomparison Project Phase 5 (CMIP5) general circulation models (GCMs) in representative concentration pathway (RCP) 4.5 and RCP 8.5 scenarios. The estimates show a temporal non-considerable increase rate of the runoff coefficient during the 21st century in both RCPs, in which the trend and uncertainty of the runoff coefficient in the dry season is projected as higher than that in the wet season. A sharp contrast between the trends of the two components of the runoff coefficient is found during the dry and wet seasons. Over the five major basins, a higher increase rate of runoff coefficient is projected in the northeastern part of the Han River basin and most of the area of the Nakdong River basin. The spatial variation in the runoff coefficient change also represents a relationship with the change in the percentage of each land cover/land use type over 109 subbasins, where the correlation of the wet-season runoff coefficient is calculated as higher than that of the dry season. This relationship is expected to vary with changes in temperature and precipitation during both seasons in three future periods.

Keywords: SWAT model; climate change; runoff coefficient; surface runoff; groundwater flow; MME analysis; water scarcity

1. Introduction

Climate change has been an increasingly popular topic in both scientific and public discourse in recent years. One of the most obvious manifestations of climate change is its influence on water balance and hydrological processes across the globe. For example, in the U.S., Chattopadhyay et al. [1,2] noted the high sensibility of hydrological response to climate variations (i.e., changes in precipitation and temperature) in the Kentucky River basin and Haw River watershed. Kumar et al. [3] reported relationships of over-proportional runoff-rainfall and under-proportional percolation-rainfall, indicating the future enhancement of floods in the Kharun catchment in India. In tropical catchments, such as Samin on Java, Indonesia, Marhaento et al. [4] found that land use change and climate change could individually cause changes in water balance components, but the changes are more pronounced in the case of combined drivers. Various studies claimed that the impact of climate change on drainage/river basins might contribute to runoff reduction in most dry tropical regions [5] while increasing runoff volume in the high latitudes and humid tropics [6,7]. Overall, climate change is considered to be the dominant factor influencing runoff over a long-term span, whereas the variations in hydrological processes in a short-term span are mainly caused by human interventions [8,9]. These impacts lead to difficulty and complication of solutions adapting to climate change and

water-related disasters, especially flooding, as it has been known as the most common and damaging hazards [10,11].

The runoff coefficient, which is influenced by not only climatic effects but also human impacts, is a fundamental indicator used in flood control, water balance, and water resources management [12,13]. This factor is contributed by two components: the surface runoff coefficient and the groundwater runoff coefficient. The surface runoff coefficient, which directly represents the ratio between the amount of surface runoff and the amount of precipitation received in a rainfall event, is a crucial parameter for flood peak discharge estimates in ungauged drainage basins [14]. The remaining component, the groundwater runoff coefficient, which can be considered to be the main contribution of the runoff coefficient, is more related to many long-term processes influenced by hydrogeological conditions [15]. This component is normally applied in determining the joint effect of the regional environmental and hydro-climatologic factors [16]. However, due to the importance of the runoff coefficient in construction plans to prevent flooding during periods of heavy rain, this coefficient is frequently considered an event-based index, focusing only on the surface runoff coefficient in most previous studies [17,18].

In recent years, a few studies have initially analyzed the change in the runoff coefficient along with studying the variability in precipitation and streamflow in some typical areas in long-term periods, but these analyses are primarily based on historical in-situ records [19–21]. In addition, the runoff coefficient normally reflects the characteristics of local topography, soil, land cover/land use, and aquifers [22]. In the case that such factors do not change, the runoff coefficient is expected to be more stable in time and space than other climatic or hydrological factors [14,18]. Based on such studies, a number of constructions regarding flood prevention or water resources management have been under development for long-term use. However, in the context of climate change, these constructions potentially become inefficient or costly solutions due to a non-thorough understanding of the runoff coefficient as a fundamental design parameter.

Meanwhile, higher temperatures are reported to increase rates of hydrologic system losses to evapotranspiration, resulting in higher annual precipitation and more frequent extreme rainfall events [23,24]. Along with the increase in the amount, the spatial and temporal distribution of precipitation is also expected to be more complicated [25]. In South Korea, the substantial difference in precipitation caused by the impact of the East Asian monsoon separates the climate into two distinct seasons: dry season (October to March) and wet season (June to September) [26,27]. This seasonal difference leads to complex variation in the runoff coefficient and its components between these two seasons, not only in the inner-annual but also in the intra-annual climate.

To overcome these challenges, numerous studies have focused on variations in water balance components under various climate change scenarios in South Korea. Jung et al. [28] found a difference in the trend of future precipitation during the dry and wet seasons, in which precipitation in the wet season increases with a higher rate than that in the dry season. Bae et al. [29,30] applied the Precipitation Runoff Modeling System (PRMS) model to analyze spatial and temporal variation in runoff and indicated that the trend of runoff is less pronounced than that of precipitation. Multiple recent studies have examined hydrological responses to the individual and combined influences of climate change and human interference. Kim et al. [31] assessed the impacts of climate change and weirs on future regional-scale runoff in the Geum River Basin and reported that climate change would lead to an increase in the future runoff ratio, while weirs contribute to an increase in minimum discharge and a decrease in maximum discharge. Lee et al. [32] indicated a regional difference in the dominant influence between climate change and human activities in the Soyang Dam upper basin and the Seom River basin.

In general, the runoff coefficient and its components have only been analyzed along with studying the behavior of precipitation and runoff in such studies using historical data. Recently, the use of the general circulation models (GCMs) output data combined with hydrological models has become one of the most effective methods to project the variation of climatic and hydrological variables. Thus, the objective of this study is to apply this method to investigate the long-term variation in the runoff

coefficient and its components in the dry and wet seasons and provide insights into the change in this coefficient in the future, which is vital for flood prevention design and construction as well as long-term water resources management to adapt to climate change in South Korea.

2. Study Area

South Korea is located at the eastern end of the Asian continent and occupies the lower half of the Korean peninsula (99,025 km²). Steep mountain ranges are distributed along the eastern coastline, while wide alluvial plains spread out to the west and south. Thus, the rivers that flow to the eastern coast are short and steep, whereas long rivers with gentle slopes discharge to the southern or western coast. South Korea is divided into five major basins: Han, Nakdong, Geum, Seomjin, and the Yeongsan River basin (Figure 1). The Han River basin is the largest basin, and the Nakdong River is recognized as the longest river, with a total length of approximately 525 km. The area of South Korea is mostly covered by forest (66%) and paddy field (18%) (Table 1). More than 90% of the agricultural land is located on slopes (>2°), and 40% of that land is located on slopes of 7°–15°.

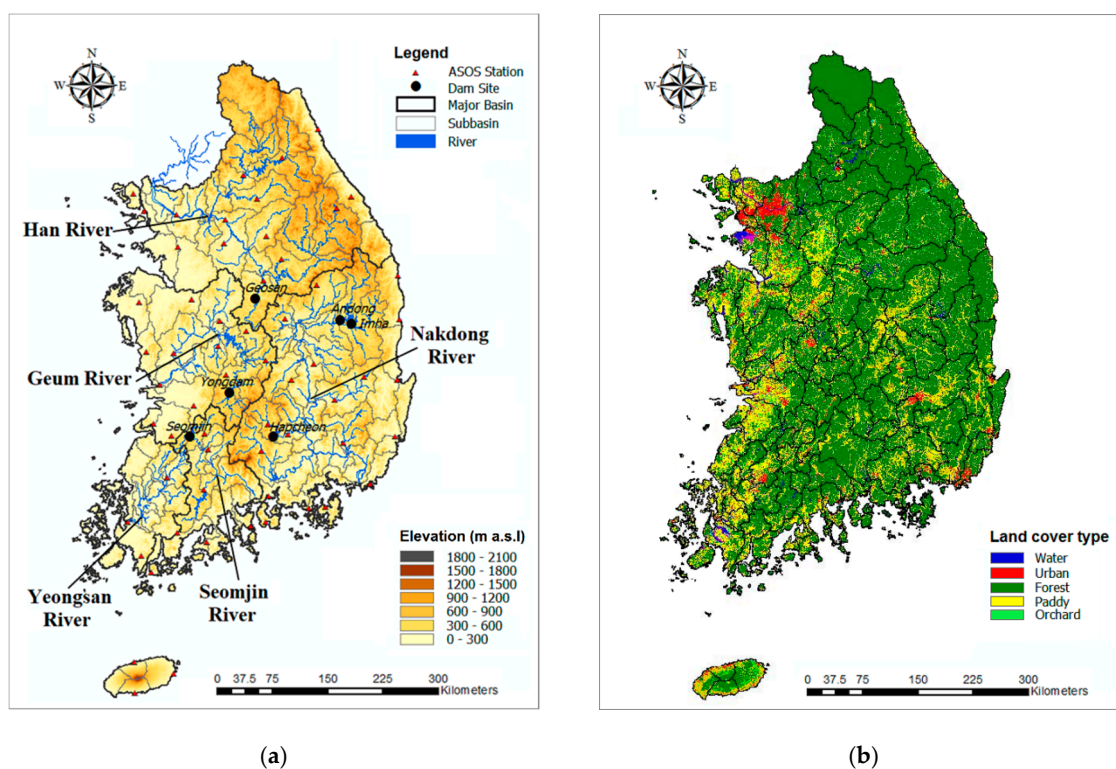


Figure 1. Characteristics of the study area: (a) topography of the catchment and locations of 5 major basins, 6 dam sites, and 60 Automated Surface Observing System (ASOS) stations; (b) land cover/land use map. (Source: digital elevation map (DEM) and land cover/land use map obtained from WAMIS; location of dams and ASOS stations obtained from KMA).

Table 1. Information on land cover/land use in the study catchment.

Basin	Total Area (km ²)	Water (%)	Urban (%)	Forest (%)	Paddy (%)	Orchard (%)	Others (%)
Han	33,808	1.22	4.13	73.44	12.84	3.68	4.68
Nakdong	31,785	0.99	2.15	71.81	15.33	9.21	0.50
Geum	17,537	2.20	5.04	52.05	25.31	9.18	6.22
Seomjin	8311	1.20	3.46	69.97	17.43	4.75	3.18
Yeongsan	7585	3.42	6.60	40.10	38.57	4.10	7.21
Total	99,025	1.49	3.79	66.28	18.21	6.55	3.68

The aquifer geology of South Korea mainly consists of crystalline rocks (granite and gneiss) and some sedimentary rocks (limestone and sandstone), which are largely formed in the Precambrian and Paleozoic eras [33]. The Precambrian metamorphic sedimentary rocks are predominantly distributed in the northern and central parts of South Korea. The Paleozoic layer is distributed in the eastern part of the Geum River basin. Relatively, large Mesozoic strata occur in the western part, in the Nakdong River basin. Quaternary alluvial deposition is narrowly distributed around large rivers or major streams.

The climate system of South Korea is driven by the effects of continental air masses during the winter and warm, humid air masses from the ocean in the summer. The annual mean temperature is 14 °C along the southern coast and then drops to 11 °C and 8 °C in the mid and northern zones, respectively. The annual rainfall distribution is determined by the dry wind from the Siberian High in the winter and the East Asia monsoon in the summer. The annual rainfall is 1274 mm, with approximately 66% received in the wet season from June to September, 16% in the transition period from April to May, and the remaining 18% in the six months of the dry season from October to March [34].

3. Materials and Methods

3.1. Hydrologic Simulation

The Soil and Water Assessment Tool (SWAT) model was developed firstly in the early 1990s by the United States Department of Agriculture, Agricultural Research Service (USDA-ARS). SWAT is a continuous-time, semi-distributed, and process-based model operating on a daily time step at the basin scale, and is well-known for its wide-application capabilities in simulating hydrological processes in large catchments using the subbasin concept under different conditions and scenarios in a long-term period [35,36]. Each catchment is divided into hydrologic response units (HRUs), integrating unique land cover/land use, soil type, and slope [37]. The HRUs are then used as the basic elements to simulate hydrological components, including evapotranspiration, surface runoff, lateral runoff, groundwater runoff, and soil water volume [35]. In the SWAT model, the simulation of the hydrological cycle is based on the water balance equation at the daily time step (Equation (1)):

$$SW_t = SW_0 + \sum_{i=1}^t (P_i - Q_i - E_i - W_i - R_i) \quad (1)$$

where SW_t (mm) is the final soil water volume, SW_0 (mm) is the initial soil water volume on day i , t (days) is the time, P_i (mm) is the precipitation amount on day i , Q_i (mm) is the amount of surface runoff on day i , E_i (mm) is the evapotranspiration amount on day i , W_i (mm) is the amount of water entering the unsaturated zone from the soil profile on day i , and R_i (mm) is the amount of return flow on day i .

For groundwater storage, the SWAT model has two main reserves, which are the shallow aquifer and the deep aquifer [38]. Water that enters the shallow aquifer from the top soil layers can either contribute to baseflow or percolate to the deep aquifer. Water stored in the shallow aquifer can also move upward to the overlying unsaturated zone by either evaporation or plant root uptake. Water in the shallow and deep aquifers can also be removed via groundwater pumping used for irrigation. The equation used to calculate the storage of groundwater in the shallow aquifer during each time step is presented in Equation (2):

$$aq_{sh,i} = aq_{sh,i-1} + w_{rchrg,sh} - Q_{gw} - w_{revap} - w_{pump,sh} \quad (2)$$

where $aq_{sh,i}$ is the amount of water stored in the shallow aquifer on day i (mm), $aq_{sh,i-1}$ is the amount of water stored in the shallow aquifer on day $i-1$ (mm), $w_{rchrg,sh}$ is the amount of recharge entering the shallow aquifer on day i (mm), Q_{gw} is the amount of baseflow entering the main channel on day i (mm), w_{revap} is the amount of revap moving into the soil zone on day i (mm), and $w_{pump,sh}$ is the amount of water removed from the shallow aquifer for consumption on day i (mm).

The rapid subsurface flow, which is significant in areas with soils having high hydraulic conductivities in the surface layers and an impermeable or semipermeable layer at a shallow depth, is taken into account based on a kinematic storage model (Equation (3)):

$$Q_{sub} = 0.024 \times \left(\frac{2 \times SW_{ly,excess} \times K_{sat} \times \sin(\alpha_{hill})}{\phi_d \times L_{hill}} \right) \quad (3)$$

where Q_{sub} (mm) is the water discharged from the hillslope outlet, $SW_{ly,excess}$ (mm) is the drainable volume of water stored in the saturated zone of the hillslope per unit area, K_{sat} is the saturated hydraulic conductivity (mm/h), α_{hill} is the slope of the hillslope segment, ϕ_d is the drainable porosity of the soil (mm/mm), and L_{hill} is the hillslope length (m).

Hydrologic simulation in SWAT involves topographic, soil, land use, and meteorological data. GIS data sets for soil type, vegetation cover, land use, and orography (Digital Elevation Model (DEM)) were obtained from the Water Resources Management Information System (WAMIS) for the current status of the study catchment and used for watershed delineation and HRU analysis. Based on the configuration of the SWAT model, the catchment was divided into 109 subbasins, with a total number of HRUs of 1551. Daily precipitation and air temperature for 60 Automated Surface Observing System (ASOS) stations (Figure 1) within the study catchment were obtained from the Korea Meteorological Administration (KMA) to compute mean areal precipitation (MAP) and mean areal temperature (MAT) for each subbasin using the Thiessen polygon method.

The daily surface runoff, groundwater runoff, and total runoff (supposed as the sum of the surface runoff and the groundwater runoff) were then accumulated for each dry and wet seasons to calculate the surface runoff coefficient, groundwater runoff coefficient, and total runoff coefficient by dividing by the corresponding accumulated precipitation.

3.2. SWAT Model Calibration, Validation, and Evaluation

In the SWAT model, numerous parameters are calibrated and validated for matching simulated and observed flows at daily time steps. The model performance was evaluated based on the coefficient of determination (R^2), Nash–Sutcliffe model efficiency coefficient (NSE) [39], root mean square error–observations standard deviation ratio (RSR) [40], and percentage bias ($PBIAS$) [41]. These indicators were calculated using Equation (4), Equation (5), Equation (6), and Equation (7), respectively:

$$R^2 = \left[\frac{n \sum_{i=1}^n S_i O_i - \sum_{i=1}^n S_i \sum_{i=1}^n O_i}{\sqrt{n(\sum_{i=1}^n S_i^2) - (\sum_{i=1}^n S_i)^2} \sqrt{n(\sum_{i=1}^n O_i^2) - (\sum_{i=1}^n O_i)^2}} \right]^2, \quad (4)$$

$$NSE = 1 - \frac{\sum_{i=1}^n (O_i - S_i)^2}{\sum_{i=1}^n (O_i - \bar{O})^2}, \quad (5)$$

$$RSR = \frac{\sqrt{\sum_{i=1}^n (S_i - O_i)^2}}{\sqrt{\sum_{i=1}^n (O_i - \bar{O})^2}}, \quad (6)$$

$$PBIAS = \frac{\sum_{i=1}^n (O_i - S_i)}{\sum_{i=1}^n O_i} \times 100, \quad (7)$$

where S_i and O_i are the simulated and observed discharge values, respectively, \bar{O} is the average observed discharge value, and n is the number of discharge values. The R^2 provides the measure of how well the model can simulate the output; the NSE shows the goodness of fit of observed and simulated data; the lower RSR , the better the model simulation performance; the $PBIAS$ analyses the trend of the observed and simulated data. The model performance is considered to be satisfactory if

$R^2 > 0.50$, $NSE > 0.50$, $RSR < 0.70$, and $-25\% < PBIAS < +25\%$. [42]. These criteria were applied to evaluate the results of the calibration and validation of the SWAT model in this study.

The SWAT model was manually calibrated and validated using observed inflow discharge provided by the WAMIS at 6 dam sites in 5 major basins of South Korea, including Geosan, Andong, Imha, Hapcheon, Yongdam, and Seomjin dams (Figure 1). Although there are many flow gauging stations in the main rivers, they are significantly influenced by upstream dam operation, so those stations were excluded from this study. Natural streamflow data, which are uncontrolled by anthropogenic structures, are required for long-term runoff analysis, are only available for selective dam sites. Hence, these data are appropriate for use in hydrologic model calibration. In addition, these dams are mostly located in the main stream of 5 major rivers; therefore, they are able to reflect the natural characteristics of streamflow in such basins.

However, there were several changes in construction planning leading to the variation in river streamflow, so it was necessary to validate the model in 2 separate periods based on the number of operational years of each dam (Table 2). After validating the SWAT model for 6 dam sites, the optimal parameter set was selected for the ungauged watersheds based on the closely related river discharge regimes using a regionalization method. This method employs a multiple regression equation, based on the configuration of basin characteristics and river discharges at a drainage basin outlet, to describe the relationship between basin geographical data and observed discharge data. The model parameters of ungauged basins were regionalized from this relationship once the correlation between observed river flows and basin characteristics of the gauged basin was calculated [30].

Table 2. Information on dams and calibration and validation periods.

Dam Site	Location		Calibration Period	Validation Period 1	Validation Period 2
	Lon (°E)	Lat (°N)			
Guesan	127.84	36.76	1996–2005	1982–1995	2006–2016
Andong	128.77	36.58	1996–2005	1977–1995	2006–2016
Imha	128.88	36.54	1999–2005	1993–1998	2006–2016
Hapcheon	128.03	35.53	1999–2005	1989–1998	2006–2016
Yongdam	127.53	35.95	2003–2005	2001–2002	2006–2016
Seomjin	127.11	35.54	1996–2005	1975–1995	2006–2016

3.3. GCM Downscaled Data Processing

3.3.1. GCM Multi-Model Data

Including other model(s) in the ensemble system is one of the most common approaches to taking uncertainty into account. The approach, in which a multitude of model simulations are grouped and compared together, is known as a multi-model ensemble (MME) analysis. This method is widely used to provide useful insights into uncertainty, where estimates of model projections are represented on the range of uncertainty. An additional advantage of MME is that each member is subjected to careful testing to obtain a credible control simulation.

To apply the MME approach in this study, 20 Coupled Model Intercomparison Project Phase 5 (CMIP5) GCM datasets at a daily scale for two representative concentration pathways (RCPs) (RCP 4.5 and RCP 8.5) representing medium and high greenhouse gas emissions, respectively, were obtained for the periods 1976–2005 (the baseline period), 2010–2039 (2030s—the early century period), 2040–2069 (2060s—the mid-century period), and 2070–2099 (2090s—the late century period). After evaluating the model performance, the downscaled and bias-corrected outputs from such models were processed individually to be input into the SWAT model to simulate hydrological processes to estimate the variation in the runoff coefficient in the future. Finally, the ensemble average of the estimated results from all the individual runs was considered to be superior to that of any single estimation.

3.3.2. Statistical Downscaling Method

The essential prerequisite to applying statistical downscaling techniques is a reliable long-term observed dataset that represents the historical range of climate events in a domain [43]. In South Korea, therefore, only 60 ASOS stations (Figure 1) providing observational meteorological variables during the long-term period from 1976 to 2005 were used to apply the statistical downscaling method.

The GCM gridded data (daily precipitation, maximum temperature, and minimum temperature) were statistically downscaled using the SDQDM method (which is known as the bias-correction/spatial disaggregation (BCSD) combined with quantile delta mapping (QDM)) for 60 ASOS stations in the historical period (30 years from 1976 to 2005) and two RCP scenarios (RCP 4.5 and RCP 8.5) from 2006 to 2099. The BCSD method comprises of two main procedures: (1) bias correction (BC) and (2) spatial disaggregation (SD). Bias-correction methods include the adjustment of mean, variance, and higher moments of a distribution by parametric [44] and non-parametric techniques [45]. Such studies have demonstrated that a non-parametric bias-correction technique, so-called quantile mapping (QM), provides higher skill systematically in reducing biases in climate models. The QDM algorithm is designed to bias-correct climate projections using QM while simultaneously preserving GCM-projected long-term changes in quantiles employing the CDF of observed data [46].

QDM is comprised of two steps in sequence: (1) calculating absolute or relative changes in quantiles between reference and future periods (Equation (8)), and (2) obtaining bias-corrected future projections by multiplying (adding for temperature) the relative changes to the historical bias-corrected value (Equation (9)).

$$\Delta_m(t) = \begin{cases} \frac{P_{m,f}(t)}{F_{m,f}^{-1}\left[F_{m,f}^{(t)}\{P_{m,f}(t)\}\right]} & \text{for precipitation} \\ T_{m,f}(t) - F_{m,f}^{-1}\left[F_{m,f}^{(t)}\{T_{m,f}(t)\}\right] & \text{for temperature} \end{cases} \quad (8)$$

$$\hat{V}_{m,f}(t) = \begin{cases} F_{o,r}^{-1}\left[F_{m,r}\{P_{m,p}(t)\}\right] \times \Delta_m(t) & \text{for precipitation} \\ F_{o,r}^{-1}\left[F_{m,r}\{T_{m,p}(t)\}\right] + \Delta_m(t) & \text{for temperature} \end{cases} \quad (9)$$

3.3.3. GCMs Performance Evaluation

The accuracy of each GCM model was statistically evaluated by comparing meteorological data generated from the GCM with observations in the baseline period. A total of 24 extreme climate indices presenting temperature and precipitation were used as evaluation factors based on the Expert Team on Climate Change Detection and Indices (ETCCDI) [43].

The Taylor diagram technique was used to evaluate the GCM performance. This diagram graphically summarizes how well the observational data (or reference value) matches the spatial patterns of the simulated data [47]. Observations and GCM data of 24 meteorological factors were visualized in the Taylor diagram. The centered root mean square error (CRMSE) and pattern correlation coefficient (PCC) from the diagram were applied as a statistical evaluation index for performance evaluation using Equation (10), Equation (11), Equation (12), and Equation (13) as follows:

$$E' = \sqrt{\frac{1}{n} \sum_{i=1}^n [(f_i - \bar{f}) - (r_i - \bar{r})]^2}, \quad (10)$$

$$R = \frac{\frac{1}{n} \sum_{i=1}^n [(f_i - \bar{f}) - (r_i - \bar{r})]}{\sigma_f \sigma_r}, \quad (11)$$

$$E'_{MME} = \frac{1}{M} \sum_{i=1}^M E'_i, \quad (12)$$

$$R_{MME} = \frac{1}{M} \sum_{i=1}^M R_i, \quad (13)$$

where, E' , E'_{MME} , R , and R_{MME} are the CRMSE and PCC of each GCM, and total model average, respectively, f_i is the GCM value, r_i is the observed value, \bar{f} is the GCM mean areal value, \bar{r} is the mean areal value of the observed data, σ_f is the standard deviation of the GCM data, σ_r is the standard deviation of the observed data, n is the total number of data, and M is the total number of GCMs.

The score of each GCM was then calculated based on a comparison between the Taylor diagram statistics and MME results for each ETCCDI factor. Ranking was determined in descending order of the total score of 24 factors. The appropriate GCMs were then selected based on the ranking, excluding GCMs where the score of the precipitation variable is not 1. Among multiple CMIP5 datasets, 13 GCMs were selected after evaluation, as listed in Table 3. The downscaled data of these models at 60 ASOS stations were then used to generate input data (MAP and MAT) for the SWAT model using the Thiessen polygon method.

Table 3. The CMIP5 general circulation model (GCM) downscaled data used in this study.

GCM	Resolution (°) (Lon × Lat)	Institution	References
CMCC-CM	0.750 × 0.748	Centro Euro-Mediterraneo sui Cambiamenti Climatici	Scoccimarro et al. [48]
CMCC-CMS	1.875 × 1.865	Centro Euro-Mediterraneo sui Cambiamenti Climatici	Bellucci et al. [49]
CESM1-BGC	1.250 × 0.942	National Center for Atmospheric Research	Lindsay et al. [50]
CNRM-CM5	1.406 × 1.401	Centre National de Recherches Meteorologiques	Voltaire et al. [51]
CanESM2	2.813 × 2.791	Canadian Centre for Climate Modelling and Analysis	Chylek et al. [52]
GFDL-ESM2G	2.500 × 2.023	Geophysical Fluid Dynamics Laboratory	Dunne et al. [53]
HadGEM2-AO	1.875 × 1.250	Met Office Hadley Centre	Collins et al. [54]
HadGEM2-ES	1.875 × 1.250	Met Office Hadley Centre	Collins et al. [54]
INM-CM4	2.000 × 1.500	Institute for Numerical Mathematics	Volodin et al. [55]
IPSL-CM5A-LR	3.750 × 1.895	Institut Pierre-Simon Laplace	Dufresne et al. [56]
IPSL-CM5A-MR	2.500 × 1.268	Institut Pierre-Simon Laplace	Dufresne et al. [56]
MRI-CGCM3	1.125 × 1.122	Meteorological Research Institute	Yukimoto et al. [57]
NorESM1-M	2.500 × 1.895	Norwegian Climate Centre	Bentsen et al. [58]

3.4. Trend Analysis

The trends in the runoff coefficient were analyzed using the Mann–Kendall trend test. The test is a non-parametric test developed for detecting trends in a time series of data. The test is widely used to analyze the trend of numerous meteorological and hydrological variables such as precipitation data [28] and streamflow data [59] at different scales. The Mann–Kendall test is not only simple and effective but also advantageous to deal with missing and below-detection-limit values.

Mann–Kendall's statistic S is computed using Equation (14) and Equation (15):

$$S = \sum_{i=1}^{n-1} \sum_{k=i+1}^n \text{sgn}(x_k - x_i), \quad (14)$$

$$\text{var}(S) = \frac{n(n-1)(2n+5) - \sum_{i=1}^m e_i(e_i-1)(2e_i+5)}{18}, \quad (15)$$

where, x_k and x_i are sequential data values; n is the length of the dataset; $\text{sgn}(\theta)$ is a sign function extracting the sign of θ , $\text{sgn}(\theta) = 1$ if $\theta > 0$, $\text{sgn}(\theta) = 0$ if $\theta = 0$, $\text{sgn}(\theta) = -1$ if $\theta < 0$; m is the number of tied groups, and e_i is the size of the i -th tied group.

S is expected to have a normal distribution with the null hypothesis H that there is no statistically significant trend carried out by the time series, and the normal value of the test Z is estimated using Equation (16):

$$Z = \frac{S - \text{sgn}(S)}{\sqrt{\text{var}(S)}} \quad (16)$$

The null hypothesis H is accepted if $-Z_{1-\alpha/2} \leq Z \leq +Z_{1-\alpha/2}$, in which, $\pm Z_{1-\alpha/2}$ are critical values and α is the significance level for the test.

In this study, the Mann–Kendall statistics and 10% and 5% significance level (with $\alpha \leq 0.10$ and $\alpha \leq 0.05$, respectively) were estimated for the total, surface, and groundwater runoff coefficients during the period 2006 to 2009. Noticeably, while the trends in precipitation and runoff can be linked to the change in climate, the trends in the runoff coefficients cannot be explained completely by the change in climate variables and, thus, a combination of climate impacts and human influences need to be considered [20].

4. Results

4.1. Evaluation of Hydrological Model Performance

The sensibility of the parameters was defined as the geometric mean of the flow rate change with respect to the increase or decrease in such parameters. A sensitivity analysis is taken for model parameters to identify the impact of each parameter on the performance of streamflow simulation. The optimal parameters and their sensibility are displayed in Table 4. The fitted value represents the ranges of the calibrated parameters among all the subbasins. Figure 2 shows a time series of the daily streamflow simulations in validation period 2 with respect to the Andong dam site on a normal scale and logarithmic scale. The results of the SWAT model performance evaluated for one calibration and two validation periods of all the dam sites are shown in Table 5.

Table 4. Sensibility of Soil and Water Assessment Tool (SWAT) model parameters.

Parameter	Definition	Range	Fitted Value	Sensibility
CN2	Runoff curve number in condition AMC-II	35–98	36–84	High
ESCO	Soil evaporation compensation coefficient of HRU	0.00–1.00	0.85–1.00	High
SOL_AWC	Effective moisture content of soils	0.00–1.00	0.00–0.27	High
GWQMN	Critical water content of the aquifer for basal outflow (mmH ₂ O)	0–5000	0	High
SOL_K	Saturated hydraulic conductivity (mm/h)	0–2000	0.9–190	Medium
GW_REVAP	Revap factor of aquifers	0.02–0.20	0.02	Medium
REVAPMN	Critical water content of aquifers averaged for revap and deep aquifers (mmH ₂ O)	0–500	1	Medium
ALPHA_BF	Groundwater (base-flow) suppression constant	0.00–1.00	0.04–0.05	Medium
GW_DELAY	Groundwater delay time (days)	0–500	31–90	Medium

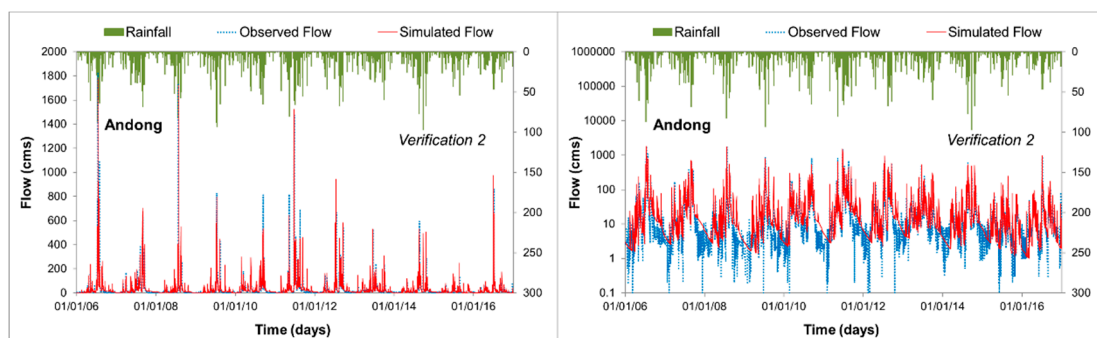


Figure 2. Comparison of streamflow simulation and observation data in the Andong dam site on a normal scale (left) and logarithmic scale (right). The green column shows the observed rainfall over the dam site, the blue dotted line shows the observed inflow discharge at the dam, and the red line shows the simulated discharge using the SWAT model.

Table 5. Calibration and validation statistics of the SWAT model for 6 dam sites.

Dam Site	Calibration Results				Validation Results 1				Validation Results 2			
	R ²	NSE	RSR	PBIAS	R ²	NSE	RSR	PBIAS	R ²	NSE	RSR	PBIAS
Guesan	0.65	0.64	0.60	−0.40	0.69	0.68	0.57	4.00	0.58	0.46	0.74	−11.70
Andong	0.84	0.81	0.43	1.10	0.79	0.79	0.46	4.10	0.74	0.72	0.53	−21.00
Imha	0.76	0.76	0.50	1.40	0.71	0.69	0.56	−6.60	0.64	0.65	0.63	−25.50
Hapcheon	0.85	0.83	0.41	2.20	0.83	0.80	0.44	−5.50	0.87	0.85	0.38	−21.50
Yongdam	0.81	0.77	0.48	−0.10	0.79	0.80	0.45	8.80	0.77	0.68	0.57	−29.10
Seomjin	0.53	0.52	0.69	−10.00	0.39	0.30	0.84	−21.40	0.74	0.70	0.55	−12.10

Overall, the evaluation shows that the performance of the model is relatively satisfactory for simulating future streamflow. The evaluation demonstrates that the SWAT model is capable of describing variations in other water balance components, including soil moisture volume and evapotranspiration, over the watershed. However, as shown in Figure 2, the behavior of the simulations has a good fit with observations in the case of high flow, while the model has difficulty capturing the characteristics of low flow in the Andong dam site. The simulation results are similar for the other dam sites.

4.2. Future Climate Predicted from the Downscale GCM Data

Projections from the GCMs show a clear warming trend in temperature in all of the months, with a significant difference between RCP 4.5 and RCP 8.5, while the change in precipitation is considerably different between the months during the dry season and during the wet season (Figure 3). The changes in monthly variables in RCP 4.5 show higher uncertainty than those in RCP 8.5, and the changes in monthly variables during the dry season show higher uncertainty than those during the wet season.

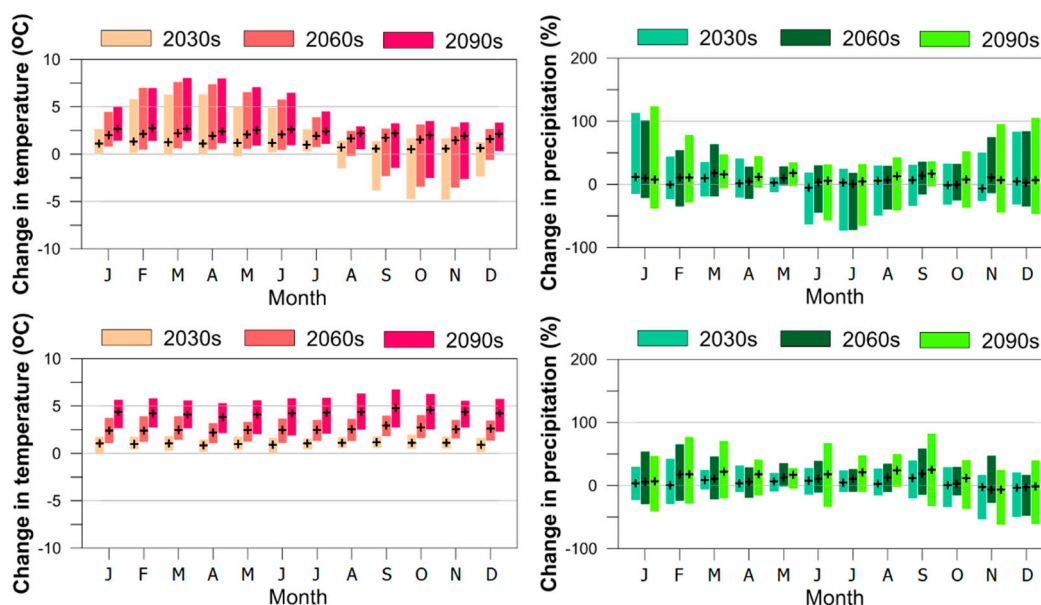


Figure 3. Changes of monthly temperature (°C) and precipitation (%) averaged from the results of 109 subbasins in 3 future periods (2010–2039, 2040–2069, and 2070–2099) referred to the baseline (1976–2005) in representative concentration pathway (RCP) 4.5 (upper half) and RCP 8.5 (lower half). The columns show the range of the change for 13 GCMs, and the black plus signs show the multi-model ensemble (MME) mean of the estimations.

In the late century, the increases in the average areal of temperature are estimated to be up to +2.341 °C and +4.302 °C in the dry season and 2.360 °C and 4.418 °C in the wet season for RCP 4.5 and RCP 8.5, respectively. During the dry season, the highest increase is found in the Han River basin, and the lowest change rate is found in the Yeongsan River basin. The regional difference in temperature

in the wet season is unnoticeable, although the Nakdong River Basin mostly shows a lower increasing rate. The change in temperature is not significantly different between the five major basins in both the dry and wet seasons, and variation in temperature change in each basin during the wet season is expected to be higher than that during the dry season (Figure 4).

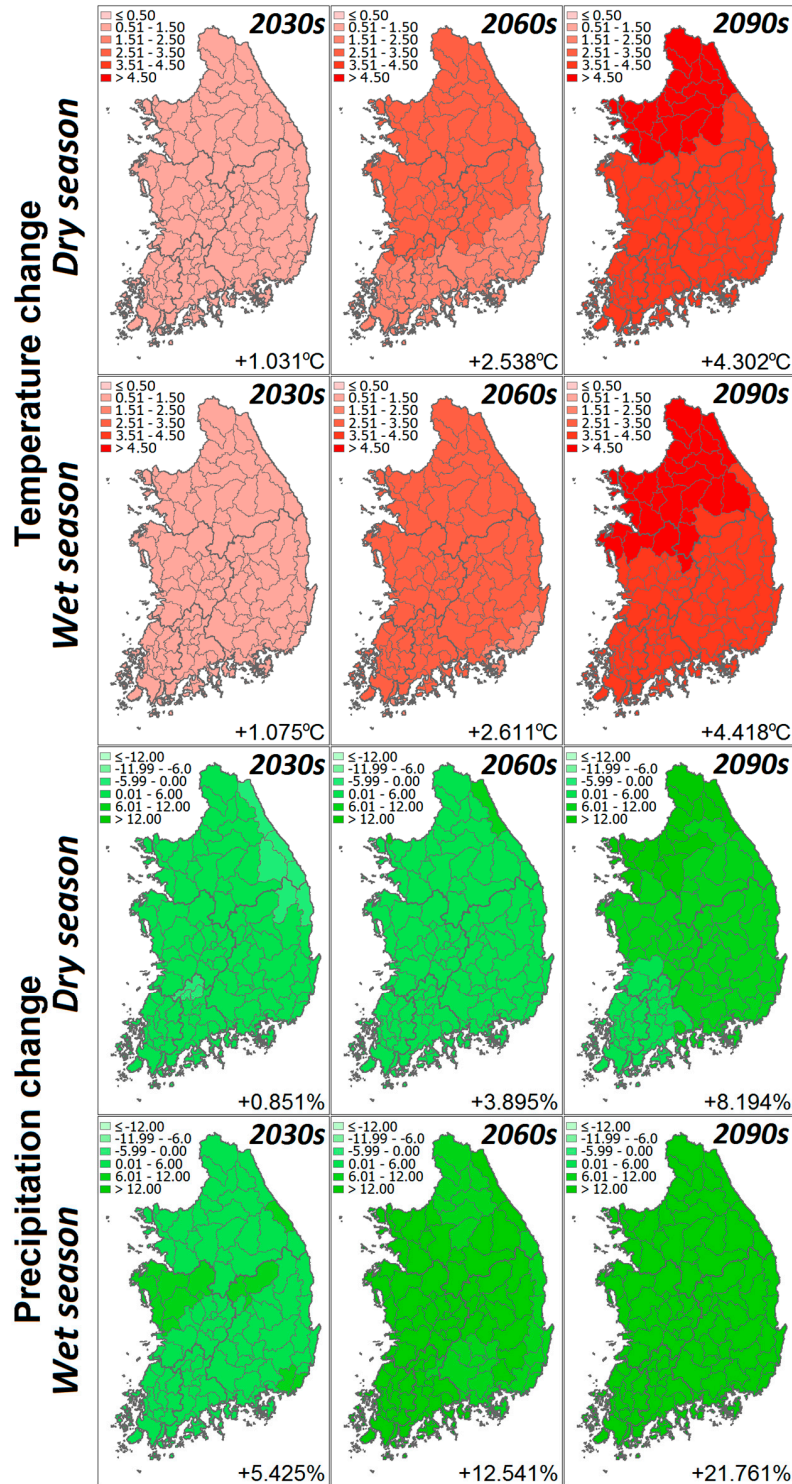


Figure 4. Spatial distribution of changes in temperature (°C) and precipitation (%) in 3 future periods (2010–2039, 2040–2069, and 2070–2099) referred to the baseline (1976–2005) in South Korea during the dry and wet seasons in RCP 8.5. The values show the MME means of downscaled results averaged for 109 subbasins.

Precipitation in the dry season is found to always increase in all future periods with no considerable difference in the regional change in both RCPs based on projected results (Figure 4). During the dry season, the projected average areal increases in precipitation in the late century are +8.557% in RCP 4.5 and +8.194% in RCP 8.5, while these values are significantly higher during the wet season, with +9.043% and 21.761% estimated for RCP 4.5 and RCP 8.5, respectively.

4.3. Temporal Trend and Uncertainty of Future Runoff Coefficient

The overall results of the trend analysis for both dry and wet seasons in South Korean basins in two RCPs are displayed in Figure 5 and Table 6. As shown in Figure 5, the runoff coefficients in the dry season have not only represented the higher increasing trend compared to that in the wet season but also expressed the higher uncertainty of simulations. Although the trends of the runoff coefficient in the dry season and in the wet season have been found to be not significantly different based on RCP 4.5, with the increasing rate expected to be approximately 0.0002/year in both seasons, in RCP 8.5, these increasing rates have become higher, and the difference between the trends of the runoff coefficient in the dry season and in the wet season has become larger, with the values estimated as 0.00057/year and 0.00039/year, respectively.

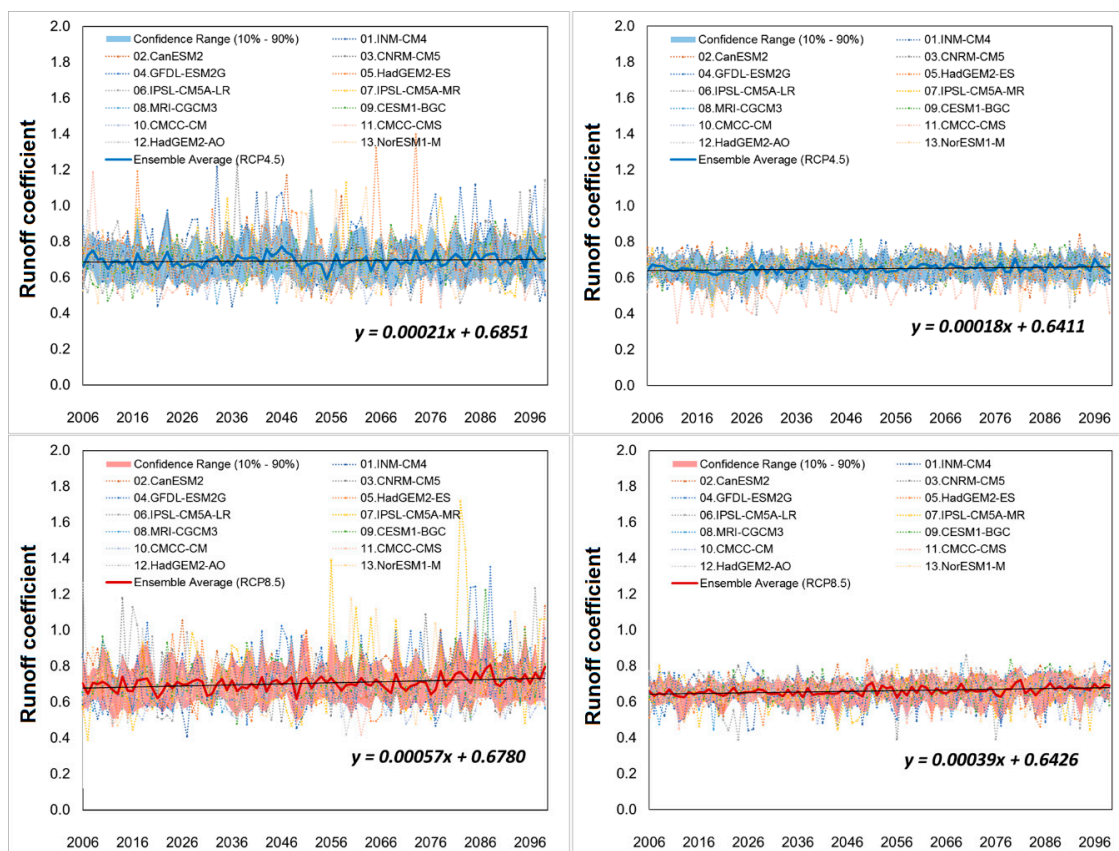


Figure 5. Trend of the runoff coefficients in the dry (left) and the wet (right) seasons in RCP 4.5 (blue) and RCP 8.5 (red). The bold lines show the ensemble averages, and the shaded areas show the confidence range (10%–90%) of the value of the total runoff coefficient averaged for 109 subbasins for each year of the period 2006–2009. The black lines show the linear regression, and the dash-dotted lines show 13 single-model estimations of the total runoff coefficient averaged for 109 subbasins for each year.

The results of the Mann–Kendall test, including the statistics *S*, the normal value *Z*, and the critical values at two significance levels, are also shown in Table 6. Referring to critical values, the results indicate that the runoff coefficient has a statistically considerable trend at the significance levels of

5% and 10% in both RCPs. A sharp contrast between the trends of two components of the runoff coefficient, as displayed in Tables 6 and 7, was expected.

Table 6. The Mann–Kendall trend test statistics of runoff coefficient and components. The trend rates are based on the multi-model ensemble mean of 13 results of the value of the change in the runoff coefficient and its components in 109 subbasins for each year of the period 2006–2009.

Scenario	Season	Runoff Coefficient	Mann-Kendall Trend Test Statistic				
			Trend Rate	S	Z	$\alpha = 0.05$	$\alpha = 0.10$
RCP 4.5	Dry	Total	0.00021	769	2.352	1.960	1.645
		Surface	−0.00011	−817	−2.665	1.960	1.645
		Groundwater	0.00028	683	2.023	1.960	1.645
	Wet	Total	0.00018	791	2.580	1.960	1.645
		Surface	0.00021	717	2.332	1.960	1.645
		Groundwater	−0.00003	−197	−0.640	1.960	1.645
RCP 8.5	Dry	Total	0.00057	693	2.260	1.960	2.576
		Surface	−0.00004	−445	−1.450	1.960	1.645
		Groundwater	0.00076	1447	4.723	1.960	1.645
	Wet	Total	0.00039	1469	4.795	1.960	1.645
		Surface	0.00063	1709	5.579	1.960	1.645
		Groundwater	−0.00024	−1583	−5.167	1.960	2.576

Table 7. Variation in the runoff coefficient and components in 3 future periods.

Scenario	Season	Runoff Coefficient	Change of Runoff Coefficient (%)		
			2010–2039	2040–2069	2070–2099
RCP 4.5	Dry	Total	3.277	4.194	5.888
		Surface	0.326	−0.961	−4.654
		Groundwater	5.124	4.298	8.423
	Wet	Total	0.250	2.161	2.659
		Surface	3.629	7.867	9.189
		Groundwater	−2.175	−2.027	−1.933
RCP 8.5	Dry	Total	3.993	6.058	9.318
		Surface	1.471	−2.875	−3.063
		Groundwater	5.129	8.606	13.841
	Wet	Total	1.724	3.458	5.239
		Surface	5.588	11.417	19.505
		Groundwater	−1.049	−2.252	−4.995

Table 7 displays the variation in the runoff coefficient and components in three future periods referred to the baseline (1976–2005). The surface runoff coefficient is estimated as strongly increasing in the wet season and decreasing in the dry season, except for the early century period, when the impacts of climate change were not very clear with relatively low increasing rates of both temperature and precipitation in the dry season in both RCP scenarios. In contrast, groundwater flow always shows an increasing trend in the dry season, but its trend always represents a negative value in the wet season in both RCPs. The surface runoff coefficient indicates the direct relationship between surface runoff and precipitation, which is closely related to the characteristics of the surface layer. When the precipitation amount and intensity increase more significantly during the wet season due to climate change, the infiltration capacity of the surface soil layer is expected to reach the final infiltration rate more rapidly, resulting in a higher surface runoff and a higher surface runoff coefficient in the wet season. In the dry season, when total runoff is mainly contributed by groundwater flow, this phenomenon does not play an important role in changing the runoff coefficient. Instead, groundwater-related factors,

such as the depth and structure of the vadose layer, have a considerable effect on the change in the runoff coefficient.

Figure 6 more clearly expresses the uncertainty of the simulation. In RCP 8.5, the highest uncertainty of the runoff coefficient is expected at the end of the 21st century; however, based on RCP 4.5, the highest uncertainty is expected in the early century, during the dry season, with the widest range defined in the 2030s. The uncertainty of the estimated runoff coefficient based on 13 GCM outputs is found to be relatively high, with the higher uncertainty defined during the dry season. This difference is found due to the dominance of the groundwater component of the runoff coefficient during the dry season, which considers a number of uncertain processes and variables mainly related to the travel time of percolating water through the vadose zone and the depth of this zone. Noticeably, the median of 30-year moving average estimations in both dry and wet seasons shows a clear fluctuation, which may refer to the impact of the interannual to decadal oscillation of climate [60].

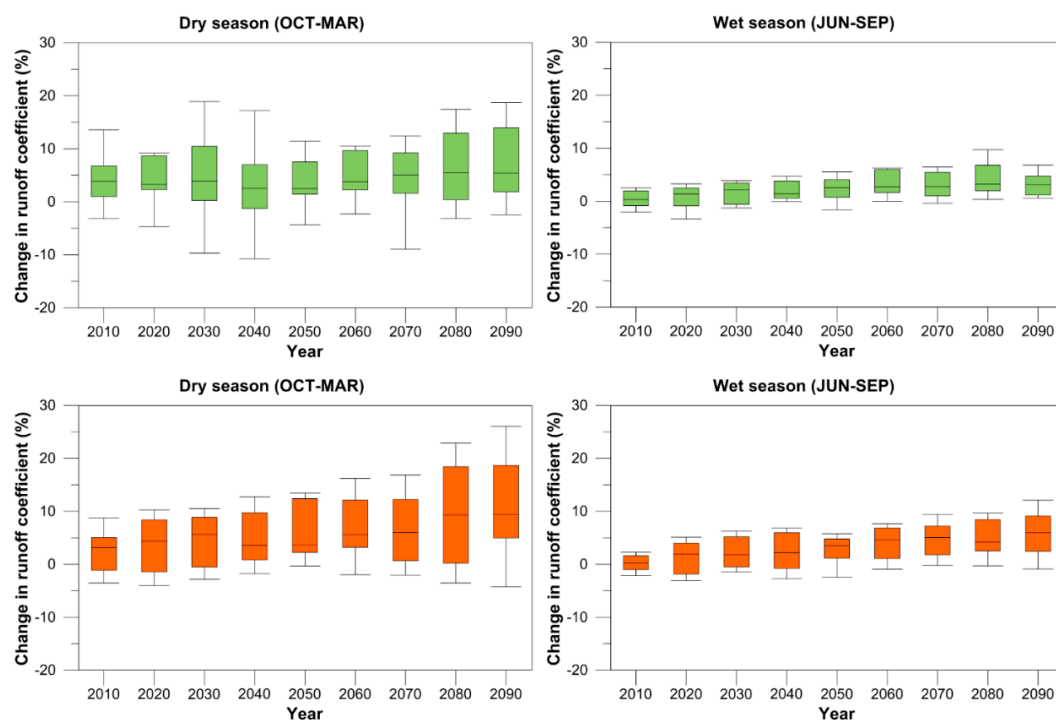


Figure 6. The 30-year moving average runoff coefficient referred to the baseline (1976–2005) during dry (left) and wet (right) seasons in RCP 4.5 (green) and RCP 8.5 (orange). The boxes show the interquartile range, the lines within the boxes show the median, and the upper and lower portions of the whiskers show the maximum and minimum estimations. The average values of the change in the runoff coefficients in 109 subbasins for each year of the period 2000–2099 are used to compute the 30-year moving average; “2010” represents the 30-year moving average of the period 2000–2019, “2020” represents the 30-year moving average of the period 2010–2029, and so on.

4.4. Spatial Distribution of Runoff Coefficient in South Korea

The spatial variation of the runoff coefficient in the dry and wet seasons is displayed in Figure 7. Particularly, in RCP 4.5, during the dry season, in the first periods, there is no significant difference in the runoff coefficient change rate between the 109 subbasins. In the next period, the northern and eastern parts of South Korea, including the northeastern part of the Han River basin and almost parts of the Nakdong River basin, have a higher change rate compared to that in other regions. This higher change rate region continues to expand and intensify in the next period, almost covering the area in northern and central South Korea. This spatial difference becomes clearer in RCP 8.5, with most areas of the Nakdong River basin showing a high increasing rate. The change in the runoff coefficient during the dry season in three future periods is different, with the highest rate estimated up to +9.318% during

the late century in RCP 8.5, and the lowest rate is +3.277% in the early century in RCP 4.5. However, during the wet season, this spatial difference is not noticeable, although the Nakdong River basin also indicates a higher increase compared to that of the other basins, the estimated average areal increases in the last period are only +2.659% and +5.239%, based on RCP 4.5 and RCP 8.5, respectively.

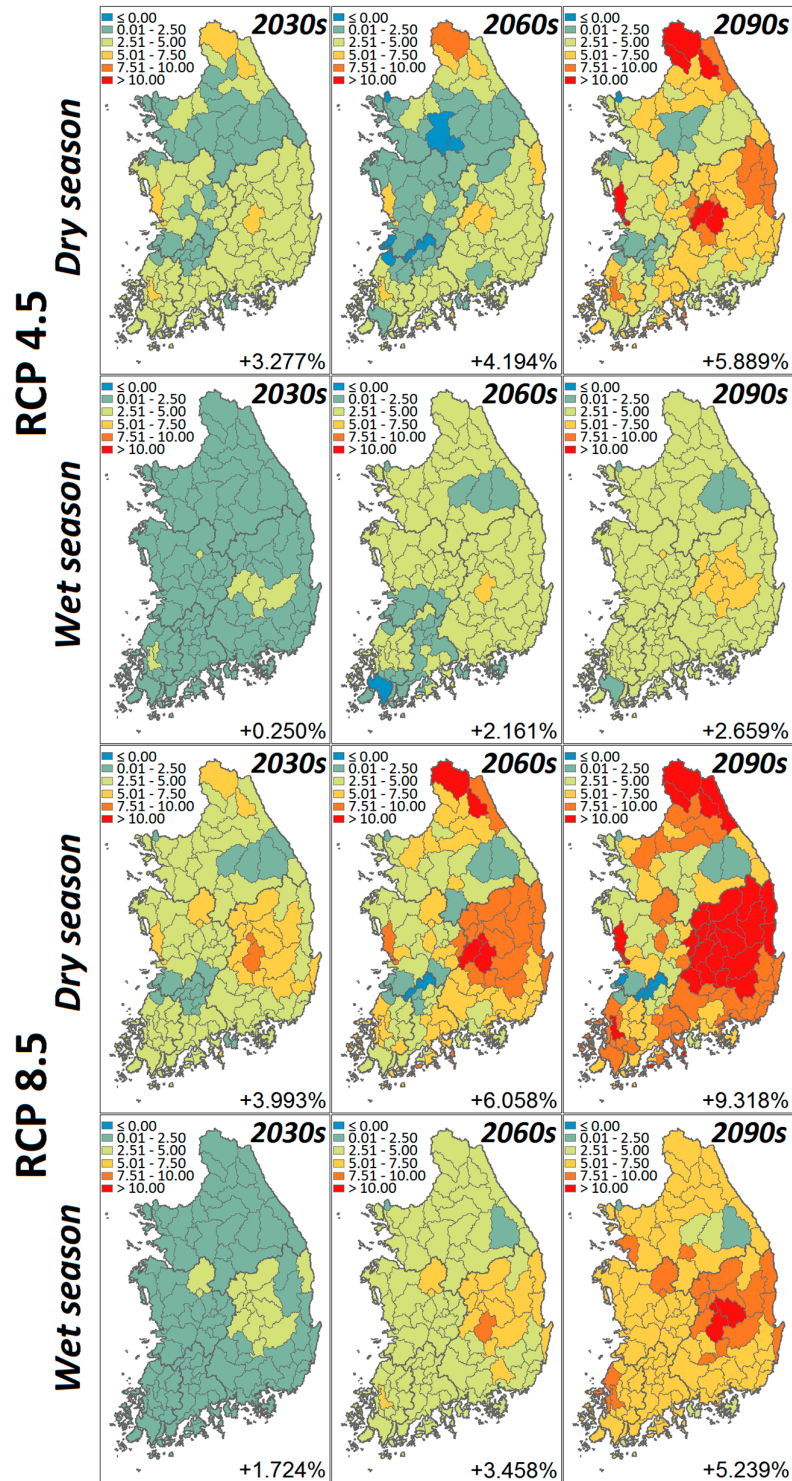


Figure 7. Spatial distribution of the runoff coefficient variation (%) in 3 future periods (2010–2039, 2040–2069, and 2070–2099) referred to the baseline (1976–2005) in South Korea during dry and wet seasons in RCP 4.5 and RCP 8.5. The values show the MME means of downscaled results averaged for 109 subbasins.

Table 8 represents the magnitude of the runoff coefficient (RC) change in terms of the ratios of important water balance components, including evapotranspiration/precipitation (ET/P—the evaporative index), surface runoff/streamflow (S/R), and baseflow/streamflow (G/R) in the dry and wet seasons in five major basins for two RCPs. This indicates that the increase in the runoff coefficient in the dry season is mainly due to the increase in groundwater runoff, whereas the increase in the runoff coefficient in the wet season mostly comes from the decrease in the evaporative index. The change rate of the total runoff coefficient is positive for three future periods, indicating that the total runoff coefficient has an increasing trend during the 21st century in both RCPs. The highest increasing rate is found in the late century based on RCP 8.5 in all basins. For the case of the Han River basin, in the dry season, the higher increase rate of the runoff coefficient may be related to the high slope of the mountainous area in the northern part and the increase in precipitation in this region. The relationship between the runoff coefficient, slope, and rainfall intensity is indicated as multivariate and nonlinear [61]. In the Nakdong River basin, this higher increase rate may be caused by the combination of soil type and human impacts, as this region is the most important paddy zone in South Korea. The existence of soil-improvement techniques and land use planning, which were partly considered via model parameters, have an effect on the water-retention capacity of the soil, in which retention parameter and saturated hydraulic conductivity are more sensitive than other parameters [62,63], with higher values of such parameters indicating greater water-retention capacity [64,65]. In addition, these impacts also contribute to reducing the amount of water used to support cultivation activities over time, contributing to the increase in the runoff during the 21st century. Streamflow, therefore, increases with the higher change rate compared to that in other regions, resulting in a higher increase rate of the runoff coefficient in three future periods.

The variation in the runoff coefficient in each of the five basins compared to the average runoff coefficient of the 109 subbasins during the dry and wet seasons in RCP 4.5 and RCP 8.5 is shown in Figure 8. Each column of the panels represents the difference in the average value of change in the runoff coefficient of the subbasins in five major river basins (Han, Nakdong, Geum, Seomjin, and Yeongsan) from the average value of the change in the runoff coefficient of the 109 subbasins referred to the baseline (1976–2005). Based on RCP 4.5, the Han River basin and the Geum River basin express a negative variation, and the Nakdong River basin exhibits a high positive variation in both the dry and the wet seasons during the 21st century. The difference in the spatial variations of the runoff coefficient among the subbasins of the Han River basin is more significant than that of other basins, followed by the Geum River basin. Based on RCP 8.5, except for the Nakdong River basin, all of the other basins represent negative variation in both the dry and the wet seasons, where the largest negative variation is found in the Geum River basin during the dry season in the late century, followed by the Seomjin River basin in the same period.

Table 8. Change in the runoff coefficients corresponding to ET/P, S/R, and G/R.

Basin	RCP	Period	ET/P				S/R				G/R				RC Change (%)	
			Ratio		Change (%)		Ratio		Change (%)		Ratio		Change (%)		Dry	Wet
			Dry	Wet	Dry	Wet	Dry	Wet	Dry	Wet	Dry	Wet	Dry	Wet	Dry	Wet
Han	RCP 4.5	2030s	0.49	0.24	2.61	-7.48	0.19	0.38	2.99	6.88	0.81	0.62	-0.69	-3.79	2.73	0.01
		2060s	0.50	0.23	3.49	-10.61	0.18	0.39	-4.16	9.18	0.82	0.61	0.97	-5.06	3.42	2.12
		2090s	0.49	0.23	1.87	-11.39	0.18	0.39	-3.94	8.78	0.82	0.61	0.91	-4.84	5.45	1.93
		2030s	0.48	0.24	0.97	-6.40	0.18	0.37	-2.02	5.57	0.82	0.63	0.47	-3.07	3.20	1.85
		2060s	0.50	0.23	5.15	-13.09	0.17	0.39	-8.04	10.65	0.83	0.61	1.86	-5.86	5.37	2.98
		2090s	0.49	0.21	2.10	-19.95	0.17	0.43	-10.16	19.66	0.83	0.57	2.35	-10.83	8.62	4.52
Nakdong	RCP 4.5	2030s	0.53	0.24	-2.08	-8.09	0.20	0.46	6.93	5.36	0.80	0.54	-1.58	-4.09	3.70	0.48
		2060s	0.52	0.23	-2.81	-11.80	0.19	0.47	2.52	7.65	0.81	0.53	-0.58	-5.83	5.05	2.81
		2090s	0.51	0.23	-4.84	-13.52	0.19	0.47	1.95	8.67	0.81	0.53	-0.44	-6.61	6.86	3.39
		2030s	0.52	0.25	-2.76	-7.50	0.19	0.45	2.02	3.83	0.81	0.55	-0.46	-2.92	5.03	2.18
		2060s	0.52	0.23	-4.04	-15.16	0.19	0.47	1.60	8.99	0.81	0.53	-0.36	-6.85	8.10	4.67
		2090s	0.50	0.21	-7.07	-21.86	0.22	0.50	-0.15	16.08	0.81	0.50	0.04	-12.25	11.86	6.25
Geum	RCP 4.5	2030s	0.46	0.25	1.47	-8.49	0.22	0.47	-0.48	6.32	0.78	0.53	0.14	-4.96	3.20	0.34
		2060s	0.47	0.25	2.18	-10.92	0.22	0.47	-4.08	7.20	0.78	0.53	1.19	-5.65	3.25	2.08
		2090s	0.46	0.25	0.74	-12.94	0.21	0.48	-8.35	8.28	0.79	0.52	2.43	-6.49	4.99	2.65
		2030s	0.46	0.26	-0.04	-6.73	0.22	0.46	-1.71	4.51	0.78	0.54	0.50	-3.54	3.66	1.98
		2060s	0.48	0.24	6.12	-14.36	0.20	0.48	-11.80	9.40	0.80	0.52	3.42	-7.37	4.99	3.58
		2090s	0.47	0.22	3.91	-21.48	0.19	0.51	-17.18	16.23	0.81	0.49	4.98	-12.73	7.37	5.38
Seomjin	RCP 4.5	2030s	0.43	0.22	-0.44	-8.94	0.23	0.51	0.94	5.83	0.77	0.49	-0.27	-5.52	2.98	0.24
		2060s	0.43	0.21	-0.40	-11.15	0.23	0.52	0.60	6.63	0.77	0.48	-0.17	-6.28	4.38	1.66
		2090s	0.43	0.21	-0.78	-13.67	0.22	0.53	-3.45	8.37	0.78	0.47	1.00	-7.92	5.45	2.27
		2030s	0.44	0.22	-0.36	-6.31	0.22	0.50	-0.20	3.11	0.78	0.50	0.05	-2.95	2.92	1.22
		2060s	0.44	0.21	1.76	-14.00	0.21	0.52	-6.35	7.81	0.79	0.48	1.84	-7.39	5.03	2.58
		2090s	0.53	0.19	1.65	-21.32	0.20	0.55	-9.19	13.98	0.80	0.45	2.66	-13.24	8.08	4.05
Yeongsan	RCP 4.5	2030s	0.53	0.27	-0.55	-8.35	0.26	0.60	-1.84	4.14	0.74	0.40	0.64	-5.55	3.72	0.49
		2060s	0.53	0.26	-1.05	-9.70	0.26	0.60	1.69	4.40	0.74	0.40	-0.60	-5.90	4.73	1.69
		2090s	0.53	0.26	-1.13	-12.44	0.25	0.61	-2.67	5.87	0.75	0.39	0.94	-0.86	5.95	2.63
		2030s	0.53	0.28	-0.74	-5.20	0.26	0.58	-1.02	2.24	0.74	0.42	0.36	-3.01	3.25	1.39
		2060s	0.54	0.26	1.67	-13.04	0.25	0.61	-4.50	5.84	0.75	0.39	1.57	-7.82	5.13	3.22
		2090s	0.54	0.23	0.41	-20.18	0.25	0.63	-2.23	10.30	0.75	0.37	0.78	-13.78	8.87	5.24

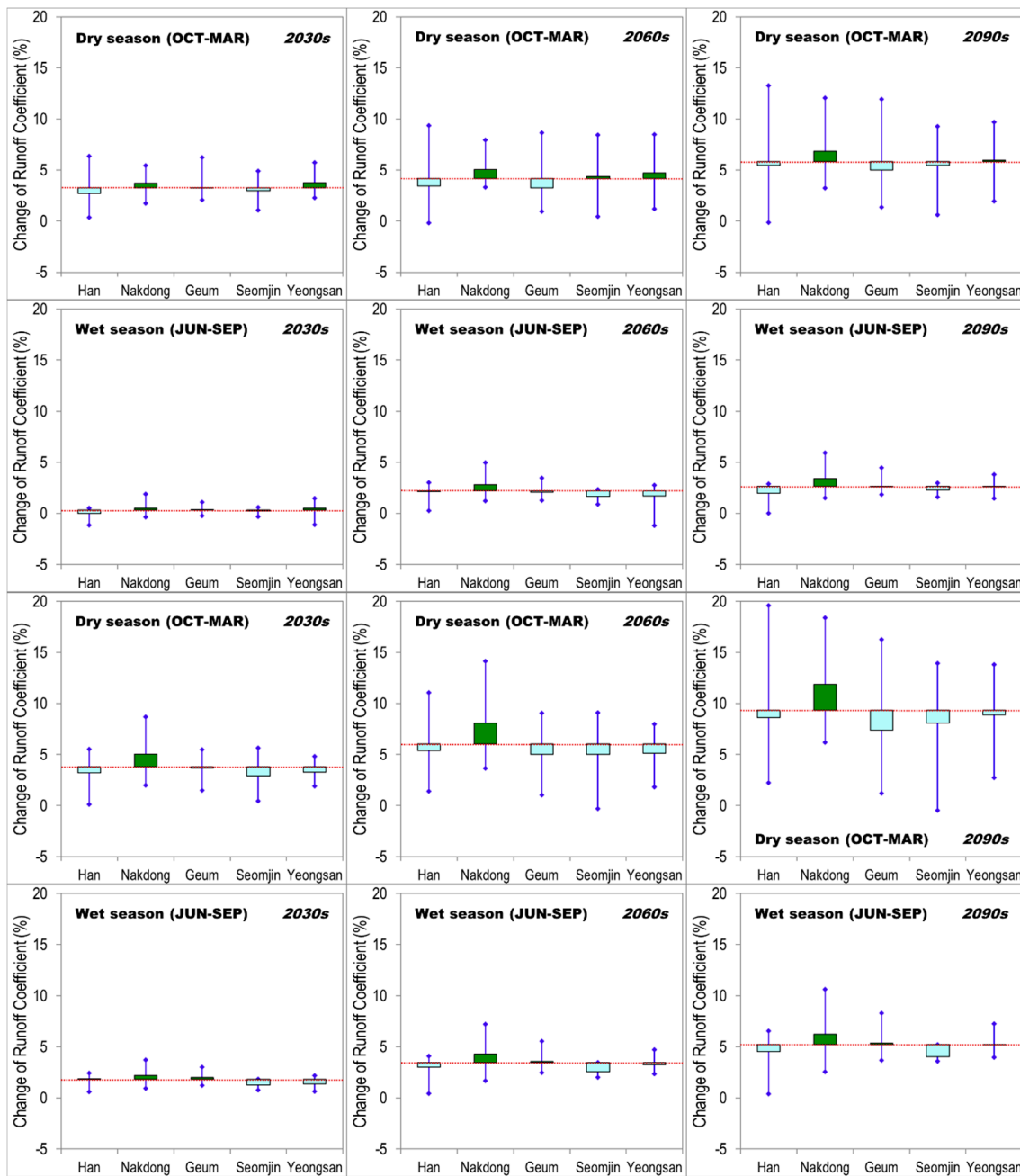


Figure 8. Runoff coefficient variations in 5 major river basins (Han, Nakdong, Geum, Seomjin, and Yeongsan) referred to the baseline (1976–2005) during the dry and wet seasons in RCP 4.5 (upper half) and RCP 8.5 (lower half). The red dotted lines show the average value of change in the runoff coefficient of 109 subbasins. The light green boxes show the negative variations (lower than the average value), and the dark green boxes show the positive variations (higher than the average value). The blue whiskers show ranges of change rates of subbasins in each major basin.

4.5. Linkage of Land Cover/Land Use and Future Runoff Coefficient Variation

Changes in the total runoff coefficient in each subbasin and the corresponding percentage of each land cover/land use type for three future periods in two RCPs (4.5 and 8.5) are shown in Table 9. These data indicate that the impact of land cover/land use on the total runoff coefficient is completely different in the dry and wet seasons. In particular, during the dry season, the total runoff coefficient shows a positive relationship with the percentage of orchard land and paddy land and a negative relationship with the percentage of forest land. In contrast, during the wet season, the total runoff

coefficient expresses a negative relationship with the percentage of orchard land and paddy land and a positive relationship with the percentage of forest land. Both seasons present a negative relationship between the total runoff coefficient and the percentage of urban (residential) land. Although land cover/land use was supposed to be unchanged during the simulation period, the change in the relationship between the total runoff coefficient and this spatial change in the land cover/land use, corresponding to the change in climate in time, should be considered for future water-related plans, as urbanization and industrialization tend to be criticized. The negative correlation between the total runoff coefficient and the percentage of urban land in both the wet and the dry seasons may predict a more serious condition of water scarcity in the future if the rate of urbanization continues to increase rapidly in South Korea.

Table 9. Correlation coefficient of the total runoff coefficient and percentage of each land use type.

Scenario	Season	Period	Urban	Forest	Paddy	Orchard
RCP 4.5	Dry	2030s	−0.068	−0.135	0.098	0.118
		2060s	−0.084	−0.102	0.069	0.218
		2090s	−0.097	−0.083	0.045	0.203
	Wet	2030s	−0.106	0.465	−0.358	−0.387
		2060s	−0.114	0.478	−0.369	−0.368
		2090s	−0.117	0.486	−0.384	−0.362
RCP 8.5	Dry	2030s	−0.068	−0.131	0.086	0.245
		2060s	−0.095	−0.097	0.053	0.266
		2090s	−0.112	−0.057	0.017	0.271
	Wet	2030s	−0.111	0.481	−0.379	−0.384
		2060s	−0.116	0.485	−0.381	−0.364
		2090s	−0.120	0.492	−0.382	−0.352

The correlation coefficient is relatively low in all cases. It is estimated to be up to +0.492, the highest value in the case of forest land during the wet season in the late century, and the lowest value in the case of paddy land during the dry season in the same period. Generally, the correlation coefficient between the total runoff coefficient and the percentage of each land cover/land use type in all the subbasins is higher during the wet season. These results indicate that the land use type strongly influences the variation in the surface runoff coefficient, contributing significantly to the variation in the total runoff during the wet season, whereas during the dry season, the total runoff coefficient is dominated by the groundwater runoff coefficient, reducing the impact of land cover/land use. However, this influence still remains, as noted by the difference in correlation of each land use type.

The impact of land cover/land use on the total runoff coefficient is found to change with the increases in temperature and precipitation in all subbasins during three future periods, as also shown in Table 9. For the case of urban land, the absolute correlation coefficient increases over the three future periods during both the dry and the wet seasons. However, there is a contrast found in the change in the absolute correlation coefficient in the dry season and in the wet season in the case of the three other land use types. The absolute correlation coefficient increases during the dry season but decreases during the wet season in the case of orchard land, whereas it decreases during the dry season but increases during the wet season in the case of forest land and paddy land. To determine the reason for this difference, the relationship between the total runoff coefficient and other climatic and hydrologic variables during the 21st century is illustrated in Figure 9 using a Taylor diagram. Variation in evapotranspiration shows a contrary correlation with the variation in the total runoff coefficient during the wet and dry seasons, and variation in the soil water volume shows a high correlation with the variation in the total runoff coefficient. As these two factors are closely related to characteristics of land cover/land use [66,67], this difference in change of correlation coefficient is expected due to the water-retention capacity of each land cover/land use type.

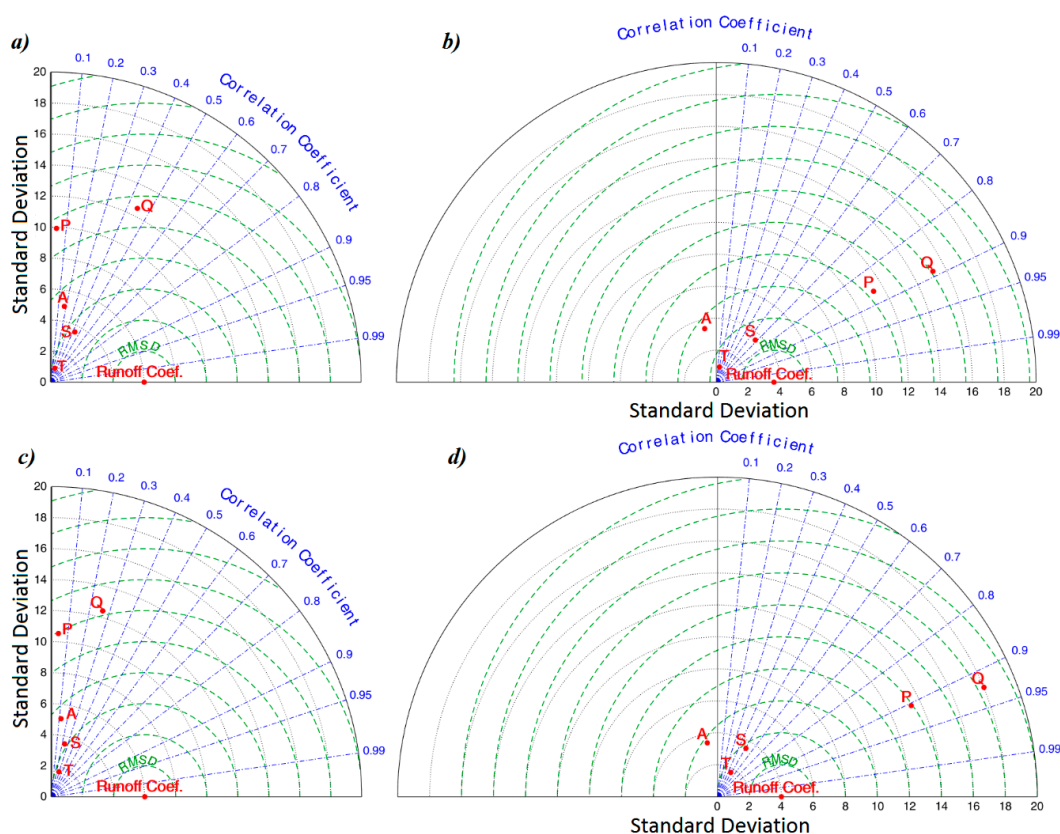


Figure 9. Taylor diagrams between the total runoff coefficient and temperature (T), precipitation (P), actual evapotranspiration (A) and soil water volume (S) during the dry (left) and wet (right) seasons in RCP 4.5 (a,b) and RCP 8.5 (c,d).

5. Discussion

Although the SWAT model shows its capacity to simulate surface runoff, groundwater flow, and total runoff, as well as other water balance components (e.g., soil moisture volume and evapotranspiration), it is limited in simulating low flow as figured out in Section 4.1. During the flood (or wet) season, when the total streamflow is relatively high, this limitation insignificantly affects simulated streamflow; nevertheless, in the dry season, it probably increases the uncertainty of simulations. This uncertainty is related to the method used for computation of the baseflow, which is normally associated with the return flow from groundwater [68,69], and to the approach used for simulation of snow melt, which is directly related to surface runoff estimation in the dry season. The poor performance impacts the estimations of groundwater runoff and dry season surface runoff, contributing to the uncertainty of the runoff coefficient in the dry season, as the amount of rainfall in this season is projected as nonsignificant. Multiple recent studies have tried to improve baseflow simulation by modifying the SWAT model regarding the aquifer structure and the interaction between aquifers [70], applying a nonlinear aquifer storage–discharge relation approach instead of the traditional approach available in the original model [71] or using a multicell aquifer to represent the regional aquifer [72]. This problem needs to be cautiously considered in further study by applying a separate baseflow separation program or improving the approach used to simulate baseflow inside the SWAT model.

The other uncertainty in the SWAT model simulations may come from the concept of HRUs, where the comprehensive parameters were calibrated and validated for each subbasin using the observed streamflow, but the parameters for the HRUs in the same subbasin are supposed to be uniform. One additional uncertainty was identified in the study of Wang et al. [73]. The study states that the impact of short-duration rainfall on streamflow could not be differentiated using the SWAT

model, leading to the high uncertainty of the runoff coefficient, but the uncertainty could be reduced by averaging for long-term periods.

The SDQDM downscaling method used in this study demonstrates its capacity to preserve the long-term trend of climatic variables, such as precipitation and minimum and maximum temperature. However, CanESM2 and IPSL-CM5A-MR models show good skills when compared for the entire Korean peninsula but propose relatively poor results on the regional scale. This may be related to the spatial resolution of the GCMs; these models could not represent the regional characteristics at each point in detail, resulting in a decrease in the regional difference of simulation results. Additionally, as found in the study of Eum and Canon [43], the SDQDM method tends to slightly overestimate the number of consecutive dry days (daily precipitation < 1 mm), and underestimate the number of consecutive wet days (daily precipitation \geq 1 mm), leading to slight underestimates of the increase in total precipitation and runoff.

The trend of temperature and precipitation in South Korea is projected to be positive during the 21st century. While the increase in temperature in the study area is considered an obvious consequence of global warming, the increase in precipitation is more related to regional effects, such as the East Asian monsoon [26,27] or Southern Oscillation [74,75]. Precipitation in the wet season shows a higher increasing trend compared to precipitation in the dry season in all basins, which is strongly related to the temporal change in the Changma front, as found in a number of previous studies [76,77]. Based on the results of the present study, the increase in precipitation due to climate change leads to a significant increase in streamflow and runoff coefficient. In particular, the increase in the runoff coefficient in the dry season was mainly due to the increase in groundwater flow, whereas the increase in the runoff coefficient in the wet season mostly came from the decrease in the evaporative index.

The increase in streamflow in rain-dominant basins results in an increase in flood frequency and intensity [28]. To develop construction plans to prevent flooding under climate change conditions in the future, the runoff coefficient is required as a critical parameter for designing. However, currently, this coefficient is only derived by traditional methods without considering the impact of climate change. Hence, the present study provides an insightful analysis of the variation in the runoff coefficient in the future, which needs to be deliberated when developing construction to adapt to climate change. Furthermore, the increase in the runoff coefficient probably predicts the decrease in the water storage capacity of the soil, leading to an increase in hydrologic drought conditions in South Korea.

On the one hand, various studies reported an increase in the surface runoff due to the increase in urban areas [78,79], resulting in the rising frequency of flood occurrences. On the other hand, it has been stated that the groundwater recharge might be reduced with the urbanization expansion because of the increase in impervious cover [80]. As a consequence, the negative correlation between the total runoff coefficient and the percentage of urban land in both the wet and dry seasons in the long-term span figured out in the present study potentially lead to the high risk of the water scarcity and flooding, especially the flash and urban floods in the future.

One of the limitations of the present study is that the temporal changes in the future of land cover/land use and other factors were not considered. However, the variation in the total runoff coefficient is potentially associated with the spatial change in land cover/land use in South Korea. Due to the combined impact of a number of soil and vegetation cover features, as well as the change in climate factors, it is difficult to identify the direct-close-clear relationship between land cover/land use and the variation in the runoff coefficient. This initial analysis suggests a correlation between spatial changes in land cover/land use and variations in the runoff coefficient in the future. This relationship would be clarified using scenarios of land use/land cover and other variable changes in further study.

6. Conclusions

The present study has examined the trend of the runoff coefficient throughout South Korea, in addition to five major basins during the future period of 2006 to 2099, and its variations in three future periods referred to the baseline (1976–2005). The results show a slightly increasing trend of the

total runoff coefficient in both the dry and the wet seasons. Specifically, the change rate of the runoff coefficient during the dry season is expected to be higher than that during the wet season. A sharp contrast was found between the trends of the two components of the runoff coefficient. Specifically, the surface runoff coefficient is projected to decrease in the dry season and strongly increase in the wet season. In contrast, groundwater runoff always shows an increasing trend in the dry season but a decreasing trend in the wet season in both RCP scenarios. This is expected due to the impact of the difference in the amount of water remaining in the surface and vadose layers on the surface runoff coefficient and groundwater runoff coefficient. A higher uncertainty of the runoff coefficient during the dry season is found due to the dominance of the groundwater component in the total runoff coefficient, as it is driven by numerous uncertain processes and variables. The results also reveal a fluctuation of the runoff coefficient during the 21st century, which is probably related to the influence of planetary oscillation on the variation in its dominant factors from the interannual to decadal scale.

Among the five major basins, the Nakong River basin is expected to have the highest increase rate of the runoff coefficient, while the lowest increase rate during the dry season is found in the Geum River basin, the lowest increasing rate during the wet season is found in the Seomjin River basin in all future periods. The difference in the spatial distribution of the runoff coefficient is associated with characteristics of soil, topographic slope, and land cover/land use in each major basin.

The variation in the total runoff coefficient shows a low correlation with the spatial change in land cover/land use over 109 subbasins; specifically, the correlation of the total runoff coefficient in the wet season is found to be higher than that in the dry season. The impact of land cover/land use on the total runoff coefficient is also found to change over time with the increase in temperature and precipitation during the 21st century. This impact is found to be different, even inconsistent, in the case of forest, orchard, and paddy land. The difference is expected due to variations in evapotranspiration and soil water volume jointly with the contribution rate of each component of streamflow.

The variation in the runoff coefficient could be very helpful for regions facing water-related issues, especially in the context of climate change. As mentioned, to develop a construction plan to prevent flooding, the runoff coefficient is required as a critical parameter for designing. However, at present, this coefficient is only derived by traditional methods without considering the impacts of climate change. Hence, the results provide an insightful analysis of variation in the runoff coefficient in the future, which needs to be considered carefully when planning or developing a construction project to adapt to climate change. Furthermore, the increase in the runoff coefficient probably predicts a decrease in the water storage capacity of the soil, leading to an increase in hydrologic drought conditions in South Korea. The outcomes of the study are not only of importance in understanding the impacts of climate change on hydrological processes and water balance for a catchment but also of significance for water resource management.

Author Contributions: Conceptualization, D.T.T.H. and D.-H.B.; methodology, D.T.T.H.; validation, D.T.T.H. and M.G.-A.; formal analysis, D.T.T.H.; resources, D.T.T.H. and D.-H.B.; data curation, D.T.T.H. and M.G.-A.; writing—original draft preparation, D.T.T.H.; writing—review and editing, D.T.T.H. and D.-H.B.; visualization, D.T.T.H. and M.G.-A.; supervision, D.-H.B.; project administration, D.-H.B.; funding acquisition, D.-H.B.

Funding: This work was supported by the Korea Environment Industry & Technology Institute (KEITI) through the Advanced Water Management Research Program, funded by the Korea Ministry of Environment (MOE). (83079).

Conflicts of Interest: The authors declare no conflict of interest.

References

1. Chattopadhyay, S.; Edwards, D.R.; Yu, Y.; Hamidisepehr, A. An Assessment of Climate Change Impacts on Future Water Availability and Droughts in the Kentucky River Basin. *Environ. Process.* **2017**, *4*, 477–507. [[CrossRef](#)]
2. Chattopadhyay, S.; Jha, M.K. Hydrological response due to projected climate variability in Haw River watershed, North Carolina, USA. *Hydrol. Sci. J.* **2016**, *61*, 495–506. [[CrossRef](#)]

3. Kumar, N.; Tischbein, B.; Kusche, J.; Laux, P. Impact of climate change on water resources of upper Kharun catchment in Chhattisgarh, India. *J. Hydrol. Reg. Stud.* **2017**, *13*, 189–207. [[CrossRef](#)]
4. Marhaento, H.; Booij, M.J.; Rientjes, T.H.M.; Hoekstra, A. Attribution of changes in the water balance of a tropical catchment to land use change using the SWAT model. *Hydrol. Process.* **2017**, *31*, 2029–2040. [[CrossRef](#)]
5. Meng, F.; Su, F.; Yang, D.; Tong, K.; Hao, Z. Impacts of recent climate change on the hydrology in the source region of the Yellow River basin. *J. Hydrol. Reg. Stud.* **2016**, *6*, 66–81. [[CrossRef](#)]
6. Karambiri, H.; García Galiano, S.G.; Giraldo, J.D.; Yacouba, H.; Ibrahim, B.; Barbier, B.; Polcher, J. Assessing the impact of climate variability and climate change on runoff in West Africa, The case of Senegal and Nakambe River basins. *Atmos. Sci. Lett.* **2011**, *12*, 109–115. [[CrossRef](#)]
7. Labat, D.; Godderis, Y.; Probst, J.L.; Guyot, J.L. Evidence for global runoff increase related to climate warming. *Adv. Water Resour.* **2004**, *27*, 631–642. [[CrossRef](#)]
8. Claessens, L.; Schoorl, J.M.; Verburg, P.H.; Geraedts, L.; Veldkamp, A. Modelling interactions and feedback mechanisms between land use change and landscape processes. *Agric. Ecosyst. Environ.* **2009**, *129*, 157–170. [[CrossRef](#)]
9. Wang, D.; Hejazi, M. Quantifying the relative contribution of the climate and direct human impacts on mean annual streamflow in the contiguous United States. *Water Resour. Res.* **2011**, *47*, W00J12. [[CrossRef](#)]
10. Arnell, N.W.; Gosling, S.N. The impacts of climate change on river flood risk at the global scale. *Clim. Chang.* **2016**, *134*, 387–401. [[CrossRef](#)]
11. Salas, J.D.; Rajagopalan, B.; Saito, L.; Brown, C. Special section on climate change and water resources: Climate nonstationarity and water resources management. *J. Water Resour. Plan. Manag.* **2012**, *138*, 385–388. [[CrossRef](#)]
12. Salazar, S.; Francés, F.; Komma, J.; Blume, T.; Francke, T.; Bronstert, A.; Blöschl, G. A comparative analysis of the effectiveness of flood management measures based on the concept of “retaining water in the landscape” in different European hydro-climatic regions. *Nat. Hazards Earth Syst. Sci.* **2012**, *12*, 3287–3306. [[CrossRef](#)]
13. Viglione, A.; Marz, R.; Blöschl, G. On the role of the runoff coefficient in the mapping of rainfall to flood return periods. *Hydrol. Earth Syst. Sci.* **2009**, *13*, 577–593. [[CrossRef](#)]
14. Giudice, D.G.; Padulano, R.; Rasulo, G. Factors affecting the runoff coefficient. *Hydrol. Earth Syst. Sci. Discuss.* **2012**, *9*, 4919–4941. [[CrossRef](#)]
15. Margat, J.; van der Gun, J. *Groundwater around the World: A Geographic Synopsis*; CRC Press/Balkema: Leiden, The Netherlands, 2013.
16. Gutry-Korycka, M. The Groundwater Runoff of Polish Rivers. *Hydrol. Res.* **1977**, *8*, 267–280. [[CrossRef](#)]
17. Blume, T.; Zehe, E.; Bronstert, A. Rainfall runoff response, event-based runoff coefficients and hydrograph separation. *Hydrol. Sci. J.* **2007**, *52*, 843–862. [[CrossRef](#)]
18. Merz, R.; Blöschl, G. A regional analysis of event runoff coefficients with respect to climate and catchment characteristics in Austria. *Water Resour. Res.* **2009**, *45*, W01405. [[CrossRef](#)]
19. Liu, L.L.; Du, J.J. Documented changes in annual runoff and attribution since the 1950s within selected rivers in China. *Adv. Clim. Chang. Res.* **2017**, *8*, 37–47. [[CrossRef](#)]
20. Velpuri, N.M.; Senay, G.B. Analysis of long-term trends (1950–2009) in precipitation, runoff and runoff coefficient in major urban watersheds in the United States. *Environ. Res. Lett.* **2013**, *8*, 24020–24026. [[CrossRef](#)]
21. Xu, Y.; Wang, S.; Bai, X.; Shu, D.; Tian, Y. Runoff response to climate change and human activities in a typical karst watershed, SW China. *PLoS ONE* **2018**, *13*, e0193073. [[CrossRef](#)]
22. Guzha, A.C.; Rufino, M.C.; Jacobs, S.; Okoth, S.; Nóbrega, R.L.B. Impacts of land use and land cover change on surface runoff, discharge, and low flows, Evidence from East Africa. *J. Hydrol. Reg. Stud.* **2018**, *15*, 49–67. [[CrossRef](#)]
23. Chou, C.; Chen, C.A.; Tan, P.H.; Chen, K.T. Mechanisms for global warming impacts on precipitation frequency and intensity. *J. Clim.* **2012**, *25*, 3291–3306. [[CrossRef](#)]
24. Trenberth, K.E. Changes in precipitation with climate change. *Clim. Res.* **2011**, *47*, 123–138. [[CrossRef](#)]
25. Kusunoki, S. Future changes in global precipitation projected by the atmospheric model MRI-AGCM3.2H with 60-km size. *Atmosphere* **2017**, *8*, 93. [[CrossRef](#)]
26. Ha, K.; Heo, K.; Lee, S.; Yun, K.; Jhun, J. Variability in the East Asian Monsoon, A review. *Meteorol. Appl.* **2012**, *19*, 200–215. [[CrossRef](#)]

27. Seo, K.; Son, J.; Lee, J.; Park, H. Northern East Asian Monsoon Precipitation Revealed by Air-mass Variability and Its Prediction. *J. Clim.* **2015**, *28*, 6221–6233. [[CrossRef](#)]
28. Jung, I.W.; Bae, D.H.; Kim, G.S. Recent trends of mean and extreme precipitation in Korea. *Int. J. Climatol.* **2010**, *31*, 359–370. [[CrossRef](#)]
29. Bae, D.H.; Jung, I.W.; Chang, H.J. Long-term trend of precipitation and runoff in Korean river basins. *Hydrol. Process.* **2008**, *22*, 2644–2656. [[CrossRef](#)]
30. Bae, D.H.; Jung, I.W.; Chang, H.J. Potential changes in Korean water resources estimated by high-resolution climate simulation. *Clim. Res.* **2008**, *35*, 213–226. [[CrossRef](#)]
31. Kim, S.; Noh, H.; Jung, J.; Jun, H.; Kim, H.S. Assessment of the Impacts of Global Climate Change and Regional Water Projects on Streamflow Characteristics in the Geum River Basin in Korea. *Water* **2016**, *8*, 91. [[CrossRef](#)]
32. Lee, S.H.; Kim, S.U. Quantification of Hydrological Responses Due to Climate Change and Human Activities over Various Time Scales in South Korea. *Water* **2017**, *9*, 34. [[CrossRef](#)]
33. Lee, J.Y.; Yi, M.J.; Yoo, Y.K.; Ahn, K.H.; Kim, G.B.; Won, J.H. A review of the national groundwater monitoring network in Korea. *Hydrol. Process.* **2007**, *21*, 907–919. [[CrossRef](#)]
34. Jayawardena, A.W.; Takeuchi, K.; Machbub, B. *Catalogue of Rivers for Southeast Asia and the Pacific Volume II*; UNESCO-IHP Publication: Hong Kong, China, 1997.
35. Neitsch, S.L.; Arnold, J.G.; Kiniry, J.K.; Williams, J.R.; King, K.W. *Soil Water Assessment Tool Theoretical Documentation Version 2000*; TWRI Report TR-191; Texas Water Resources Institute: College Station, TX, USA, 2002.
36. Ruan, H.W.; Zou, S.B.; Yang, D.W.; Wang, Y.H.; Yin, Z.L.; Lu, Z.X.; Li, F.; Xu, B.R. Runoff Simulation by SWAT Model Using High-Resolution Gridded Precipitation in the Upper Heihe River Basin, Northeastern Tibetan Plateau. *Water* **2017**, *9*, 866. [[CrossRef](#)]
37. Arnold, J.G.; Srinivasan, R.; Williams, J.R. Large area hydrologic modeling and assessment. Part I, Model development. *J. Am. Water Resour. Assoc.* **1998**, *34*, 73–89. [[CrossRef](#)]
38. Neitsch, S.L.; Arnold, J.G.; Kiniry, J.R.; Williams, J.R. *Soil and Water Assessment Tool Theoretical Documentation Version 2009*; TWRI Report TR-406; Texas Water Resources Institute: College Station, TX, USA, 2011.
39. Nash, J.E.; Sutcliffe, J.V. River flow forecasting through conceptual models, Part I-A discussion of principles. *J. Hydrol.* **1970**, *10*, 282–290. [[CrossRef](#)]
40. Golmohammadi, G.; Prasher, S.; Ali Madani, A.; Ramesh Rudra, R. Evaluating Three Hydrological Distributed Watershed Models: MIKE-SHE, APEX, SWAT. *Hydrology* **2014**, *1*, 20–39. [[CrossRef](#)]
41. Sorooshian, S.; Duan, Q.; Gupta, V.K. Calibration of rainfall-runoff models: Application of global optimization to the Sacramento Soil Moisture Accounting Model. *Water Resour. Res.* **1993**, *29*, 1185–1194. [[CrossRef](#)]
42. Moriasi, D.; Arnold, J.; Van Liew, M.; Bingner, R.; Harmel, R.; Veith, T. Model evaluation guidelines for systematic quantification of accuracy in watershed simulations. *Trans. ASABE* **2007**, *50*, 885–900. [[CrossRef](#)]
43. Eum, H.I.; Cannon, A.J. Intercomparison of projected changes in climate extremes for South Korea: Application of trend preserving statistical downscaling methods to the CMIP5 ensemble. *Int. J. Climatol.* **2017**, *37*, 3381–3397. [[CrossRef](#)]
44. Piani, C.; Weedon, G.P.; Best, M.; Gomes, S.M.; Viterbo, P.; Hagemann, S.; Haerter, J.O. Statistical bias correction of global simulated daily precipitation and temperature for the application of hydrological models. *J. Hydrol.* **2010**, *395*, 199–215. [[CrossRef](#)]
45. Gudmundsson, L.; Bremnes, J.B.; Haugen, J.E.; Engen-Skaugen, T. Technical note: Downscaling RCM precipitation to the station scale using statistical transformations; a comparison of methods. *Hydrol. Earth Syst. Sci.* **2012**, *16*, 3383–3390. [[CrossRef](#)]
46. Cannon, A.J.; Sobie, S.R.; Murdock, T.Q. Bias correction of GCM precipitation by Quantile mapping, How well do methods preserve changes in quantiles and extremes? *J. Clim.* **2015**, *28*, 6938–6959. [[CrossRef](#)]
47. Taylor, K.E. Summarizing multiple aspects of model performance in a single diagram. *J. Geophys. Res.* **2001**, *106*, 7183–7192. [[CrossRef](#)]
48. Scoccimarro, E.; Gualdi, S.; Bellucci, A.; Sanna, A.; Fogli, P.G.; Manzini, E.; Vichi, M.; Oddo, P.; Navarra, A. Effects of Tropical Cyclones on Ocean Heat Transport in a High Resolution Coupled General Circulation Model. *J. Clim.* **2011**, *24*, 4368–4384. [[CrossRef](#)]
49. Bellucci, A.; Gualdi, S.; Masina, S.; Storto, A.; Scoccimarro, E.; Cagnazzo, C.; Fogli, P.; Manzini, E.; Navarra, A. Decadal climate predictions with a coupled OAGCM initialized with oceanic reanalyses. *Clim. Dyn.* **2012**, *40*, 1483–1497. [[CrossRef](#)]

50. Lindsay, K.; Bonan, G.B.; Doney, S.C.; Hoffman, F.M.; Lawrence, D.M.; Long, M.C.; Mahowald, N.M.; Moore, J.K.; Randerson, J.T.; Thornton, P.E. Preindustrial control and 20th century carbon cycle experiments with the earth system model CESM1 (BGC). *J. Clim.* **2014**, *27*, 8981–9005. [[CrossRef](#)]
51. Voldoire, A.; Sanchez-Gomez, E.; Salas y Méliá, D.; Decharme, B.; Cassou, C.; Sénési, S.; Valcke, S.; Beau, I.; Alias, A.; Chevallier, M.; et al. The CNRM-CM5.1 global climate model—Description and basic evaluation. *Clim. Dyn.* **2012**, *40*, 2091–2121. [[CrossRef](#)]
52. Chylek, P.; Li, J.; Dubey, M.; Wang, M.; Lesins, G. Observed and model simulated 20th century arctic temperature variability: Canadian earth system model CanESM. *Atmos. Chem. Phys. Discuss.* **2011**, *11*, 22893–22907. [[CrossRef](#)]
53. Dunne, J.P.; John, J.G.; Adcroft, A.J.; Griffies, S.M.; Hallberg, R.W.; Shevliakova, E.; Stouffer, R.J.; Cooke, W.; Dunne, K.A.; Harrison, M.J.; et al. GFDL’s ESM2 Global Coupled Climate–Carbon Earth System Models. Part I, Physical Formulation and Baseline Simulation Characteristics. *J. Clim.* **2012**, *25*, 6646–6665. [[CrossRef](#)]
54. Collins, W.J.; Bellouin, N.; Doutriaux-Boucher, M.; Gedney, N.; Halloran, P.; Hinton, T.; Hughes, J.; Jones, C.D.; Joshi, M.; Liddicoat, S.; et al. Development and evaluation of an Earth-System model-HadGEM2. *Geosci. Model. Dev.* **2011**, *4*, 1051–1075. [[CrossRef](#)]
55. Volodin, E.M.; Dianskii, N.A.; Gusev, A.V. Simulating present-day climate with the INMCM4.0 coupled model of the atmospheric and oceanic general circulations. *Izv. Atmos. Ocean. Phys.* **2010**, *46*, 414–431. [[CrossRef](#)]
56. Dufresne, J.L.; Foujols, M.A.; Denvil, S.; Caubel, A.; Marti, O.; Aumont, O.; Balkanski, Y.; Bekki, S.; Bellenger, H.; Benshila, R.; et al. Climate change projections using the IPSL-CM5 earth system model-From CMIP3 to CMIP5. *Clim. Dyn.* **2013**, *40*, 2123–2165. [[CrossRef](#)]
57. Yukimoto, S.; Adachi, Y.; Hosaka, M.; Sakami, T.; Yoshimura, H.; Hirabara, M.; Tanaka, T.; Shindo, E.; Tsujino, H.; Deushi, M.; et al. A new global climate model of the meteorological research institute: MRI-CGCM3—Model description and basic performance. *J. Meteorol. Soc. Jpn.* **2012**, *90*, 23–64. [[CrossRef](#)]
58. Bentsen, M.; Bethke, I.; Debernard, J.B.; Iversen, T.; Kirkevåg, A.; Seland, O.; Drange, H.; Roelandt, C.; Seirstad, I.A.; Hoose, C.; et al. The Norwegian earth system model, NorESM1-M Part 1—Description and basic evaluation of the physical climate. *Geosci. Model. Dev.* **2013**, *6*, 687–720. [[CrossRef](#)]
59. Solander, K.C.; Bennett, K.E.; Middleton, R.S. Shifts in historical streamflow extremes in the Colorado River Basin. *J. Hydrol. Reg. Stud.* **2017**, *12*, 363–377. [[CrossRef](#)]
60. Scafetta, N. Solar and planetary oscillation control on climate change: Hind-cast, forecast and a comparison with the CMIP5 GCMs. *Energy Environ.* **2013**, *24*, 455–496. [[CrossRef](#)]
61. Mu, W.; Yu, F.; L, C.; Xie, Y.; Tian, J.; Liu, J.; Zhao, N. Effects of Rainfall Intensity and Slope Gradient on Runoff and Soil Moisture Content on Different Growing Stages of Spring Maize. *Water* **2015**, *7*, 2990–3008. [[CrossRef](#)]
62. Malone, R.W.; Gene, Y.; Baffaut, C.; Gitau, M.; Qi, Z.; Amatya, D.M.; Parajuli, P.B.; Bonta, J.V.; Green, T. Parameterization Guidelines and Considerations for Hydrologic Models. *Trans. ASABE* **2015**, *58*, 1681–1703.
63. Stratton, B.T.; Sridhar, V.; Gribb, M.M.; McNamara, J.P.; Narasimhan, B. Modeling the spatially varying water balance processes in a semiarid mountainous watershed of Idaho. *J. Am. Water Resour. Assoc.* **2009**, *45*, 1390–1408. [[CrossRef](#)]
64. Liu, L.; Zhang, R.; Zuo, Z. The Relationship between Soil Moisture and LAI in Different Types of Soil in Central Eastern China. *J. Hydrometeorol.* **2016**, *17*, 2733–2742. [[CrossRef](#)]
65. Yang, H.; Piao, S.; Huntingford, C.; Ciais, P.; Li, Y.; Wang, T.; Peng, S.; Yang, Y.; Yang, D.; Chang, J. Changing the retention properties of catchments and their influence on runoff under climate change. *Environ. Res. Lett.* **2018**, *13*, 094019. [[CrossRef](#)]
66. Dias, L.C.P.; Márcia, N.M.; Marcos, H.C.; Michael, T.C.; Christopher, N. Effects of land cover change on evapotranspiration and streamflow of small catchments in the Upper Xingu River Basin, Central Brazil. *J. Hydrol. Reg. Stud.* **2015**, *4*, 108–122. [[CrossRef](#)]
67. Niu, C.Y.; Musa, A.; Liu, Y. Analysis of soil moisture condition under different land uses in the arid region of Horqin sandy land, northern China. *Solid Earth* **2015**, *6*, 1157–1167. [[CrossRef](#)]
68. Bosch, D.D.; Arnold, J.G.; Volk, M.; Allen, P.M. Simulation of a low-gradient coastal plain watershed using the SWAT landscape model. *Trans. ASABE* **2010**, *53*, 1445–1456. [[CrossRef](#)]

69. Guse, B.; Reusser, D.E.; Fohrer, N. How to improve the representation of hydrological processes in SWAT for a lowland catchment—Temporal analysis of parameter sensitivity and model performance. *Hydrol. Process.* **2014**, *28*, 2651–2670. [[CrossRef](#)]
70. Luo, Y.; Arnold, J.G.; Allen, P.; Chen, X. Baseflow simulation using SWAT model in an inland river basin in Tianshan mountains, Northwest China. *Hydrol. Earth Syst. Sci.* **2012**, *16*, 1259–1267. [[CrossRef](#)]
71. Wang, Y.; Brubaker, K. Implementing a nonlinear groundwater model in the soil and water assessment tool (SWAT). *Hydrol. Process.* **2014**, *28*, 3388–3403. [[CrossRef](#)]
72. Nguyen, V.T.; Dietrich, J. Modification of the SWAT model to simulate regional groundwater flow using a multicell aquifer. *Hydrol. Process.* **2018**, *32*, 939–953. [[CrossRef](#)]
73. Wang, H.; Sun, F.; Xia, J.; Liu, W. Impact of LUCC on streamflow based on the SWAT model over the Wei River basin on the Loess Plateau in China. *Hydrol. Earth Syst. Sci.* **2017**, *21*, 1929–1945. [[CrossRef](#)]
74. Jin, Y.H.; Kawamura, A.; Jinno, K.; Berndtsson, R. Detection of ENSO-influence on the monthly precipitation in South Korea. *Hydrol. Process.* **2005**, *19*, 4081–4092. [[CrossRef](#)]
75. Lee, S.; Kwon, W.T. A variation of summer rainfall in Korea. *J. Geol. Soc. Korea* **2004**, *39*, 819–832.
76. Chung, Y.S.; Yoon, M.B.; Kim, H.S. On climate variations and changes observed in South Korea. *Clim. Chang.* **2004**, *66*, 151–161. [[CrossRef](#)]
77. Ho, C.H.; Lee, J.Y.; Ahn, M.H.; Lee, H.S. A sudden change in summer rainfall characteristics in Korea during the late 1970s. *Int. J. Climatol.* **2003**, *23*, 117–128. [[CrossRef](#)]
78. Miller, J.D.; Hutchins, M. The impacts of urbanisation and climate change on urban flooding and urban water quality: A review of the evidence concerning the United Kingdom. *J. Hydrol. Reg. Stud.* **2017**, *12*, 345–362. [[CrossRef](#)]
79. Du, J.; Change, L.; Zhang, Q.; Yang, Y.; Xu, W. Different Flooding Behaviors Due to Varied Urbanization Levels within River Basin: A Case Study from the Xiang River Basin, China. *Int. J. Disaster Risk Sci.* **2019**, *10*, 89–102. [[CrossRef](#)]
80. Wakode, H.B.; Baier, K.; Jha, R.; Azzam, R. Impact of urbanization on groundwater recharge and urban water balance for the city of Hyderabad, India. *ISWCR* **2018**, *6*, 51–62. [[CrossRef](#)]



© 2019 by the authors. Licensee MDPI, Basel, Switzerland. This article is an open access article distributed under the terms and conditions of the Creative Commons Attribution (CC BY) license (<http://creativecommons.org/licenses/by/4.0/>).